ISTANBUL TECHNICAL UNIVERSITY ★ INSTITUTE OF SCIENCE AND TECHNOLOGY

ELECTROCHEMICAL DEPOSITION AND CRYSTAL QUALITY ENHANCEMENT OF COPPER INDIUM DISELENIDE

M.Sc. THESIS

Serkan GÜRBÜZ

Department of Chemistry

Chemistry Programme

MAY 2014

ISTANBUL TECHNICAL UNIVERSITY ★ INSTITUTE OF SCIENCE AND TECHNOLOGY

ELECTROCHEMICAL DEPOSITION AND CRYSTAL QUALITY ENHANCEMENT OF COPPER INDIUM DISELENIDE

M.Sc. THESIS

Serkan GÜRBÜZ
(509111063)

Department of Chemistry

Chemistry Programme

Thesis Advisor: Prof. Dr. A. Sezai SARAÇ

MAY 2014

İSTANBUL TEKNİK ÜNİVERSİTESİ ★ FEN BİLİMLERİ ENSTİTÜSÜ

ELEKTROKİMYASAL YÖNTEMLE BAKIR İNDİYUM DİSELENÜR SENTEZİ VE KRİSTAL KALİTESİNİN ARTIRILMASI

YÜKSEK LİSANS TEZİ

Serkan GÜRBÜZ
(509111063)

Kimya Anabilim Dalı

Kimya Programı

Tez Danışmanı: Prof. Dr. A. Sezai SARAÇ

MAYIS 2014

Serkan Gürbüz, a **M.Sc.** student of ITU **Institute of Science and Technology** student ID **509111063**, successfully defended the **thesis** entitled "**ELECTROCHEMICAL DEPOSITION AND CRYSTAL QUALITY ENHANCEMENT OF COPPER INDIUM DISELENIDE**", which he prepared after fulfilling the requirements specified in the associated legislations, before the jury whose signatures are below.

Thesis Advisor :	**Prof. Dr. A. Sezai SARAÇ** İstanbul Technical University	.....
Jury Members :	**Prof. Dr. Süleyman AKMAN** İstanbul Technical University	.....
	Prof. Dr. Yücel ŞAHİN Yıldız Technical University	.....

Date of Submission : 05 May 2014
Date of Defense : 26 May 2014

To my spouse,

FOREWORD

I would like to thank my advisor, Prof. Dr. A. Sezai SARAÇ, for his guidance and scientific discussions for my research and to establish my thesis as a well-studied subject. As well, I would like to thank my advisor for his understanding and patience during my researh period.

I would like to thank Dr. Melek EROL, Dr. Sema MEMİŞ, Dr. Cemil DIZMAN and Dr. Şerife SARIOĞLAN for their support on this subject with chemicals they supplied for me.

I would like to thank Dr. Figen TÜRKSOY for her kind permission to use the equipment.

I would like to thank my group members also especially Zeliha GÜLER, Burcu SAYINLI, Dilek SUADİYE and Timuçin BALKAN for their efforts.

Finally, I would like to thank my wife Gülnur DERELİ GÜRBÜZ for her support within the time of my research and thesis.

May 2014

Serkan GÜRBÜZ
Chemist

TABLE OF CONTENTS

Page

ABBREVIATIONS

CIS	**:** Cooper Indium Diselenide
CIGS	**:** Cooper Indium Gallium Diselenide
XRD	**:** X-Ray Diffraction
SEM	**:** Scanning Electron Microscope
TEM	**:** Transmission Electron Microscope
AFM	**:** Atomic Force Microscopy
EDS	**:** Energy Dispersive X-Ray Spectroscopy
CdTe	**:** Cadmium Telluride
a-Si	**:** Amorphous Silicon
CdS	**:** Cadmium Sulfide
ZnO	**:** Zinc Oxide
DSC	**:** Dye-sensitized Solar Cells
OPV	**:** Organic Photovoltaics
P3HT	**:** Poly 3-hexylthiophene
PCBM	**:** Phenyl-C_{61}-butyric acid methyl ester
PEDOT:PSS	**:** Poly(3,4-ethylenedioxythiophene) Polystyrene sulfonate
AAS	**:** Atomic Absorption Spectroscopy
XRF	**:** X-Ray Fluorescence Spectroscopy
SCE	**:** Saturated Calomel Electrode
FWHM	**:** Full Width at Half Maximum
MSE	**:** Mercury Sulfate Electrode
KSCN	**:** Potassium Thiocyanate
FTIR	**:** Fourier Transform Infrared Spectroscopy

LIST OF TABLES

Page

LIST OF FIGURES

Page

ELECTROCHEMICAL DEPOSITION AND CRYSTAL QUALITY ENHANCEMENT OF COPPER INDIUM DISELENIDE

SUMMARY

Nowadays solar cells supply 2.6% of the total energy consumption of Europe. In our country, energy produced from solar cells, despite having more sunny days, is 0.1 W per person, which is well below the average of Europe. Therefore, research has to be done on solar cells and new solar technologies have to be produced. In literature, instead of Silicon based solar cells there is a common diversion towards thin film technologies. From thin film technologies CIS and CIGS, which have % 20.8 photo conversion efficiency, have % 2 of total share from solar panel sales. CIS and CIGS are good candidates to conduct a research on rather than less toxic other alternative thin film technologies (CdTe).

Adsorbing material of CIS/CIGS solar cells either produced at low temperatures with electrochemistry or at high temperature with vapor deposition techniques. In literature and commercially CIS/CIGS grown with electrochemistry is polycrystalline and has to be heated at high temperatures to improve crystal quality of the material. However, because of different expansion coefficients of the absorbing material, metal contacts and substrates, thin film is being damaged. As well, use of flexible substrates, which is a promising material, is very hard with these methods.

We studied to overcome these problems by synthesizing high crystal quality material at electrodeposition step with several optimization procedures. High crystal quality CIS semiconductor with electrochemical technique was synthesized. An X-Ray diffraction (XRD) based approach was done with several parameter optimizations such as salt concentrations, deposition potential and acidity of the solution. As-deposited samples were characterized with XRD, SEM, EDAX, AFM and optical microscope techniques. Crystallite size increase up to 17.31 nm was achieved by increasing the acidity of the deposition solution. In addition to common tetragonal phase of CIS, a new phase for electrodeposition of CIS, wurtzite, was assigned which was thought to compete with tetragonal phase at electrodeposition.

ELEKTROKİMYASAL YÖNTEMLE BAKIR İNDİYUM DİSELENÜR SENTEZİ VE KRİSTAL KALİTESİNİN ARTIRILMASI

ÖZET

Günümüzde güneş pilleri Avrupa'nın enerji ihtiyacının yüzde 2,6'sını sağlamakta ve bu oran her yıl hızlıca artmaktadır. İstatiksel veriler güneş pillerinden üretilen enerjinin oranının yıllık % 42 oranında arttığını ve güneş enerjisinin tüm yenilenebilir enerji kaynakları arasında en yüksek artış oranına sahip enerji kaynağıdır.

Teorik olarak bakıldığında ise hali hazırda dünyada yüksek oranda kullanılan yenilenebilir enerji kaynaklarından biyokütle ve rüzgâr enerjisine nazaran binlerce kat daha fazla potansiyele sahiptir. Özellikle nüfus artışıyla birlikte biyokütle gibi enerji kaynaklarına tarım arazilerinden dolayı azalma olması beklenmektedir. Bu nedenlerden dolayı dünyada hızla gelişen güneş enerjisi pazarına özellikle yıllık güneşli gün sayısının fazla olmasından dolayı Türkiye'nin de girmesi kaçınılmazdır.

Güneş pilleri sektöründe silis esaslı ürünler yıllardan beri çalışılmakta olup bu tipteki piller için verimlilik artışı beklenmemektedir. Özellikle silis elementinin güneş pilleri için yüksek saflıkta hazırlanması için gereken yüksek sıcaklıklar ve harcanan enerji bu tipteki güneş panellerinin maliyetlerini artırmaktadır. Bu yüzden daha az madde gerektiren ve daha kolay koşullarda elde edilebilen ince filmlerin araştırması dünyada hızla ilerlemektedir.

Bu çalışmalar arasında bakır indiyum galyum diselenür (CIGS) şu ana kadar elde edilen % 20,8 foto verimlilik ile öne çıkmaktadır. Bir güneş pili için kullanılan madde kalınlığı bu tarz ince filmler için 1-2 mikron kalınlığında olmakla birlikte silis esaslı pillere göre (250 mikron) çok daha az miktardadır.

CIGS ve bakır indiyum diselenür (CIS) fiziksel veya kimyasal buhar kaplama yöntemleri ile sentezlenmektedir. Fakat bu yöntem yüksek sıcaklıklar ve yüksek maliyetli cihazlar içerdiğinden ticarileşme açısından bakıldığında pahalı bir tekniktir. Alternatif olarak elektrokimyasal olarak yarı-iletkenler sentezlenmektedir. CIS/CIGS elektrokimyasal olarak polikristal halinde oda sıcaklığında sentezlenebilmektedir. Elektrokimyasal üretim ile beraber bu malzemelerin fabrikasyonu için gerekli ekipmanlar için anapara maliyetleri ve kullanılan hammadde maliyetleri önemli oranda düşmektedir.

Günümüzde CIGS güneş pili üreten firmaların önemli bir kısmı daha ucuz maliyetli olan elektrokimyasal yöntem ile üretimi tercih etmiştir. Aynı zamanda elektrokimyasal tekniğin düşük sıcaklıkta uygulanabilmesi makaradan makaraya sisteminin kullanılması ve esnek tabanlı malzemelerin kullanımına imkân sağlamaktadır. Tüm bu avantajları göz önünde bulundurarak elektrokimyasal CIGS üretimi üzerinde yoğunlaşılması gereken önemli bir konudur.

Elektrokimyasal CIGS üretiminin vakum yöntemlerine göre en büyük dezavantajı elde edilen malzemenin düşük kristal özelliğe sahip polikristal veya amorf halde elde edilmesidir. Sonrasında ise termal ısıtma ile maddenin kristal kalitesinin artırılması gerekmektedir. Fakat gerek farklı genleşme katsayıları ve gerek karmaşık yapıda olmasından dolayı oluşan komplesitesi güneş pilinin vakum yöntemleri kadar yüksek verimlerde olmamasına yol açmaktadır. % 20'lerde olan vakum metodu ile elde edilen foto verimlilik, elektrokimya ile elde edilen % 15 foto verimlilikten yeterince fazla miktardadır.

Aynı zamanda esnek taban diye nitelendirilen polimerik altlıkların kullanımı elektrokimya esnasında düşük kristal kalitesinde madde elde edilmesi ve sonrasında termal ısıtma işleminin uygulanmak zorunda olmasından dolayı sorun yaratmaktadır. Polietilen gibi ticari olarak kolay elde edilebilen, yaygın polimerlerin kullanımı, düşük camsı geçiş sıcaklıklarından dolayı neredeyse imkânsızdır. Daha dayanıklı polimit gibi esnek tabanlar üzerinde durulan ve birçok çalışmanın yapıldığı esnek taban adaylarıdır. Fakat bu altlıkların camsı geçiş sıcaklıkları 500 °C altında olduğundan termal ısıtma işlemi tam olarak yapılamamakta ve verim kayıpları oluşmaktadır.

Bu yüzden elektrokimya esnasında kristal kalitesinin yeterince artırılması durumunda termal ıstma işlemine gerek kalmayacak veya daha düşük sıcaklıklarda yapılabilecektir. Bu sayede yüksek verimli pillerde polimerik esnek tabanların kullanımına imkân sağlanacak ve daha da önemlisi maliyetli ısıtma işlemleri ortadan kalkacağından oluşturulacak piller daha ucuz maliyetle üretilebilecektir.

Kristal kalitesinin artırılması işlemi elektrokimya esnasında kaplanan maddenin kaplama çözeltisi içerisinde çözünürlüğünü artırarak sağlanılacağı önerilmiş ve bu çalışmanın sonuncunda daha yüksek kristal kalitesinde filmler elde edilmiştir. Literatürde CdS gibi yarıiletkenlerin çözünürlüğü çözeltinin asitliği arttıkça yükseldiği bilinmektedir. Bu durumda CIS için de aynı durumun söz konusu olacağı ve daha düşük pH değerlerinde çözünürlüğünün artacağı öngörülmüş ve bu çözünen kısımların kristalin amorf kısımlarından olacağı öngörülmüştür. Elektrokimyasal kaplama işlemi devam ettiğinden kristal bir yandan amorf kısımlarından daha fazla olmak üzere çözünecek ve diğer taraftan devam eden kaplama ile oluşan kristal büyüyecek ve daha büyük kristaller elde edilebilecektir.

Çalışmada öncelikle CIS için kaplama parametreleri taranmış ve en uygun koşullar bulunmuştur. Ardından çözeltinin pH değeri değiştirilerek farklı kaplamalar yapılmıştır. Sonuç olarak asitlik arttıkça kristal boyutunun büyüdüğü X-ışını kırınımı metodu ve Debye Scherrer formülü ile gösterilmiştir. Literatürdeki ortalama değerler 1-5 nm kristal boyutlarına tekabül etmekteyken yapılan deneyler sonrasında 1,09 pH değerinde 17,71 nm kristal boyutunda parçacıklar elde edilmiştir.

Aynı zamanda literatürde sıklıkla gözlemlenen fakat tam olarak neden olduğu bilinmeyen 25,2 2θ değerindeki pikin wurtzite fazındaki CIS yarı iletkeninden gelebileceği öngörülmüştür. CIS büyümesi hem $Cu_{2-x}Se$ hem de In_2Se_3 bileşiklerinden olduğu yorumlanmıştır. Bu pikin In_2Se_3 bileşiğinden geldiği düşünülmüş fakat bu bileşiğin bazı piklerinin eksik olmasından kesin sonuca varılamamıştır. Çalışmamızda ise daha yüksek kristal kalitesinde ince film elde edilmesiyle pikler daha keskin olduğundan pikler daha ayrı biçimde bulunmuş ve farklı parametrelerin taranmasıyla 28,5 2θ değerinde başka bir pik varlığı ile bu bileşiğin esasında wurtzite CIS olabileceği tahmin edilmiştir. Literatürde bu faz nanoparçacıklar için gözlemlenmiş olup elektrokimya deneylerinde rastlanılmamıştır.

CIS büyümesi $Cu_{2-x}Se$ bileşiğinden tetragonal yapıda büyümesi ve In_2Se_3 bileşiğinden wurtzite yapıda büyümesi olarak düşünülmüştür. Bu bileşiklerle son fazların kafes parametrelerinin yakın olmasından ötürü bu şekilde bir büyüme olabileceği düşünülmektedir. EDS analizleri de bu tezi doğrulamakta ve SEM görüntülerinden toplanmış ve düz yüzeylerin analizinde toplanmış kısımlarda bakır/indiyum oranı fazla çıkmakta ve düz kısımlarda ise daha az çıkmaktadır. Bu sonuç düz yüzey için iki farklı bileşikten ziyade wurtzite tek fazı ihtimalini kuvvetlendirmektedir.

Elde edilen kaplamalar SEM, EDS, AFM ve optik mikroskop ile de analiz edilmiş ve morfolojileri, pürüzlülükleri ve kompozisyonları analiz edilmiştir.

1. INTRODUCTION

Copper indium gallium diselenide (CIGS) is the leader of the thin film technologies with significant rise at efficiencies recent years [1]. Efficiencies more than 20 % were achieved by laboratory scale solar cells [2]. Thin film solar cells have higher potential on the photovoltaic market due to reduced cost per unit area and no need for expensive substrates or high process temperatures [3]. As well miscibility of these compounds allows synthesis of quaternary alloys with desired band gap with respect to stoichiometric ratios [3]. Large light absorption coefficient of CIGS/CIS semiconductors gives the advantage of less material usage [3]. Typical thicknesses of a few micrometers are enough for CIGS photovoltaic cell [4].

CIGS has the same growth processes as CIS and therefore understanding properties of CIS has direct impact on CIGS thin film technologies. CIS (or CIGS) can be grown with many techniques including co-evaporation [5] and sputtering [6].

Electrodeposition is also a widely used technique [7-16] with advantage of lower capital and lower energy requirements, as well as roll-to-roll process compatibility [17]. However, material obtained by electrodeposition is polycrystalline [11,18] or amorphous [10,19]. Therefore, the deposited film has to be annealed at high temperatures which limit the efficiency of the cells prepared with flexible polymeric substrates [3,20].

To overcome this problem and reduce the cost we aim to increase the crystallinity of the films, which was targeted by Lincot et al. [21], as much as possible at electrodeposition step. This can be applicable for more acidic conditions with taking advantage of increased solubility [22-23] of the deposit itself in the deposition solution and dissolving from amorphous sites and recrystallize again with ongoing electrodeposition finally resulting higher crystallinity. We adapted trending pulsed electrodeposition method [24-29] for our experiments.

1.1 Experimental Techniques

1.1.1 Pulsed Electrodeposition

In pulsed electrodeposition the potential is changed between two different values as shown in Figure 1.1. This results a series of pulses with same duration and amplitude. Pulses consist of on and off time intervals. Depending on the pulse parameters such as potenatials and on-off time it is possible to control film composition and thickness of the deposit.

In electroplating a negatively charged layer is formed around cathode. This layer makes it harder for ions to reach cathode. In pulsed electrodeposition by switching off the potential applied, this layer is discharged and ions move more easily at the next pulse period. By using pulses ion depletion zones are eliminated and ion deposit more uniform on the surface [30].

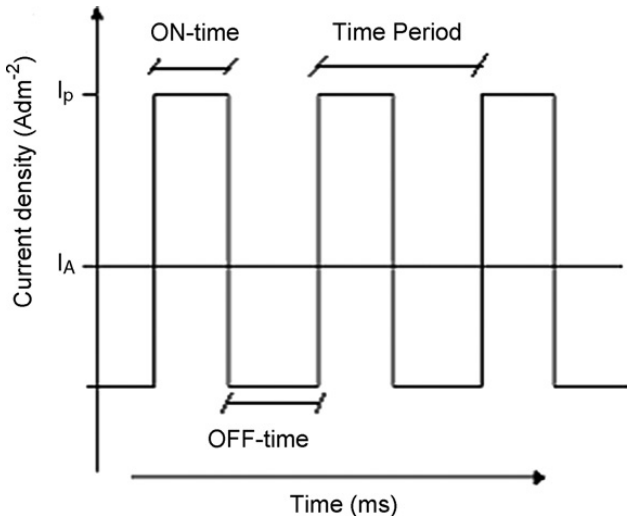

Figure 1.1 : Example of pulses at pulsed electrodeposition [30].

1.1.2 X-Ray Diffraction

X-Rays generated from an X-Ray tube are used to understand crystalline properties of the material being analyzed. Typically, X-Rays are formed after radiation of the Tungsten filament and exposure to a metal to produce characteristic X-Rays. Most of the X-Ray tubes include copper as X-Ray generator. Cu Kα X-Rays having wavelength of 1.54 Å are formed by this way. These X-Rays are used to analyze the sample. Only diffracted X-Rays satisfying Bragg's Law ($n\lambda=2d\sin\theta$) are counted by the detector. Diffraction of the X-Ray beams are shown in Figure 1.2. By analyzing

the diffracted beams atomic or molecular positions, composition, crystallinity and grain size of the material can be found [31].

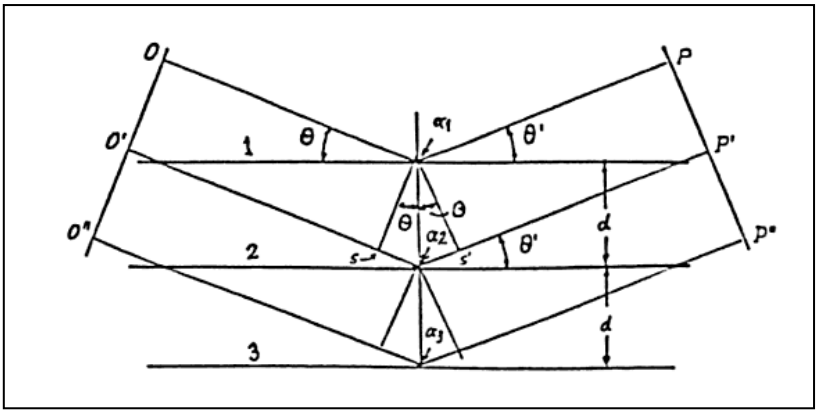

Figure 1.2 : Diffraction of the X-Ray beams from the sample [31].

1.1.3 Scanning Electron Microscope

Scanning electron microscope uses focused beam of electrons to visualize a sample. Electrons focus on very small field on the sample. These eletrons interact with the sample to produce signals that can be detected and give information about the topography of the sample. The instrument invented by Manfred von Ardenne in 1930s. Most commonly secondary electrons mode are used to give better information of the surface. Moreover, defects or voids can also be observed with the aid of a scanning elecron microscope. Resolution of the instrument can go down to 1 nm.

To visualize a sample with SEM, sample must be conductive. If not, specimen is covered with conductive metal such as gold or palladium with using a sputter or an evaporator. Typical operating voltages are between 1 kV to 30 kV.

1.1.4 Energy Dispersive Spectroscopy

EDS uses X-Rays for excitation of the elements present in the sample. Each element has its own response to the X-Ray resulting from the K and L electron shell of the sample elements. To measure characteristic response of the elements specimen is trgeted with a high energy beam of electrons or X-Rays.

These beams cause electron transfer from the inner shell to the outer shell of the element. This act creates an empty electron hole at the inner shell in most cases ground level shell. Electron from outer shell may fill this hole and energy difference

between two shells are released as characteristic X-Rays which can be measured by EDS equipment for elemental analysis.

1.1.5 Atomic Force Microscopy

By using a mechanical probe surface is scanned fast with the aid of piezoelectric elements. A sharp tip is used to scan the specimen surface. Such tips can be either Silicon or Silicon Nitride with having tip radius dimensions of nanometer scale. When the tip approaches the surface, it is repelled according to Hooke's Law. A constant force is adjusted at the scanning of the surface to eliminate the risk of breaking of the tip. Three different modes can be applied as contact, tapping and non-contact modes.

1.1.6 Optical Microscope

Optical microscope is used to magnify objects illuminated with visible light and the aid of system of lenses. Optical microscope is among the oldest imaging techniques and alternative to SEM and TEM. Maximum magnification achieved by an optical microscope is 1000x obtained by eyepiece and objective lenses. Many illumination techniques such as bright field, dark field, cross polarized light and phase contrast can be used to get better view. Optical microscope technique give informtion about the focused surface. High roughness samples usually are mixed with focused and defocused zones.

1.1.7 Fourier Transform Infrared Spectroscopy

FTIR is a technique to obtain infrared spectrum of the sample either solid, liquid or gas. FT term is Fourier Transform and comes form the transformation of the raw data into actual spectrum. Absorption of the light by the sample is measured and these characteristic wavelength responses are used for analysis. Such specific absorptions are the result of molecular vibration of the bonds.

1.2 Solar Cells

Crystalline silicon and multicrystalline solar cells hold % 80 of the total photovoltaic market. Rest is covered by CdTe, CIGS and a-Si based photovoltaic cells. Bulk Si photovoltaics take advantage of advanced growth and fabrication processes. More than 20 % power conversion efficiencies achieved by Si solar panels approach to the

28 % theoretical conversion efficiency. As well, because of bulk Si wafer price, solar panel costs can not be decreased enough to compete with the potential costs of the thin film technologies[3,20,32].

Market share of CdTe based solar panels reached to 12.3 % with doubling its share in the recent years. Thin film solar panels have advantage of less material usage because of higher absorption coefficients. As well, they have direct transitions unlike indirect transitions of Si solar cells. 30 % maximum efficiency is calculated from the optimum band gap range of 1.2-1.4 eV of the absorbing material. CdTe (1.44 eV) and CI(G)S (1.02-1.6 eV) fits well in this range as shown in the Figure 1.3 below.

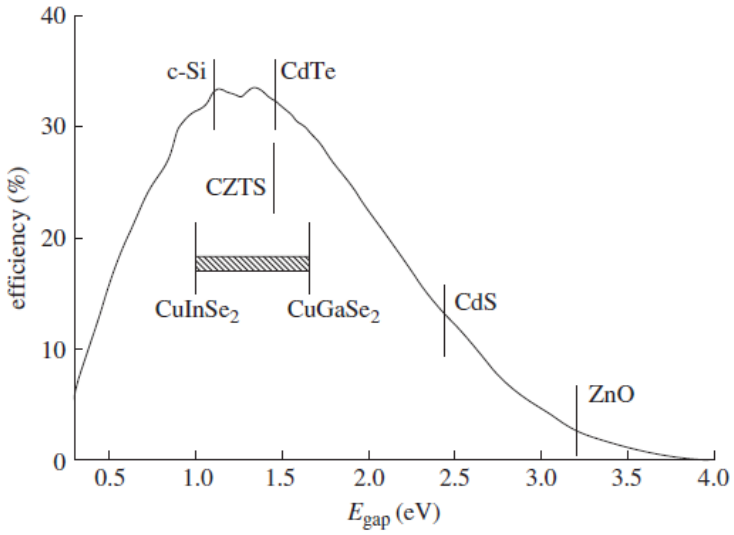

Figure 1.3 : Optimum band gap – theoretical efficiency calculation graph [32].

Solar cells make rapid progress in the recent years reaching two-third of the quasi limit of the theoretical cell. In the Table 2.1 below, maximum efficiencies obtained by each type of photovoltaic cell is given progressively [1].

1.2.1 CdTe Thin Film Solar Cells

CdTe having 1.44 eV band gap lies in the middle of the optimum band gap. Large light absorption coefficient of the material ensures 99 % of the incident photons with energies larger than the band gap is absorbed by the material. 2 micron thick CdTe is enough for the maximum light absorption. Efficiencies up to 16.5 % for research cells and 10-11 % module cells were obtained by CdTe based thin film solar cells. CdTe based thin film solar cells are cheap as it was assumed 0.52-0.63 $ Wp by 2014 [3,20,32].

Table 2.1 : Best research solar cell efficiencies table [1].

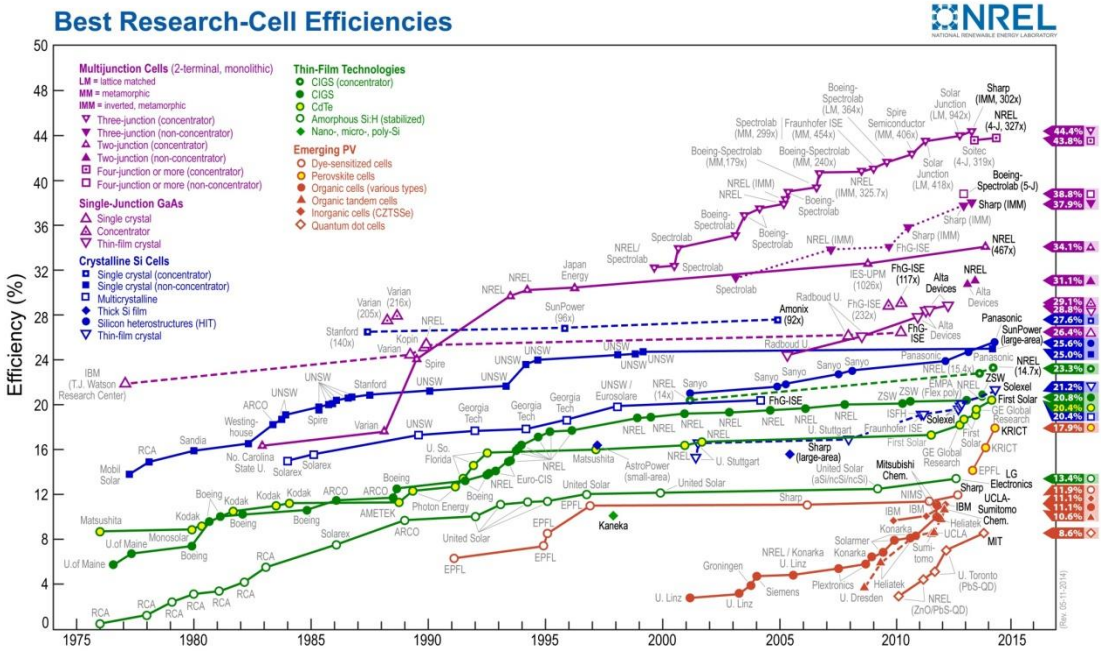

As illustrated in the Figure 1.4 below, solar cell consist of 2-5 micron thick CdTe absorbing layer, 50 nm thick CdS buffer layer and ZnO window layer. CdS buffer layer was kept thin to avoid absorption at CdS and maximize absorption of CdTe.

Back contact of the cell is problematic because work function matching cheap metal is unavailable.

The main issue of CdTe based solar cells is toxicity of the Cadmium and abundance of the Tellurium. Therefore, progress of CdTe based solar cells may slow down in the future.

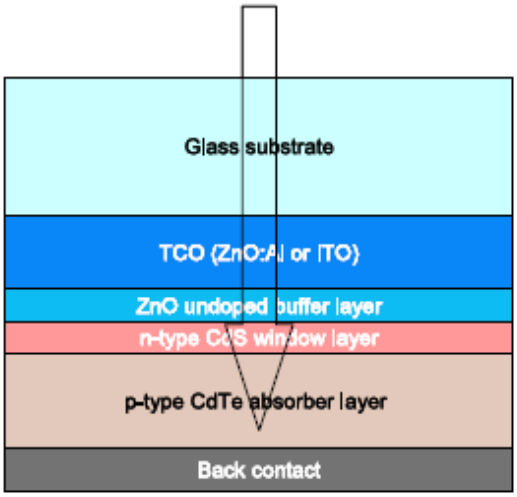

Figure 1.4 : Typical CdTe solar cell [3].

1.2.2 CI(G)S Thin Film Solar Cells

Large light absorption coefficients of the CI(G)S layer allow a micron of material is enough for maximum light absorption. Power conversion efficiencies more than 20 % were achieved for research cells and module cells up to 13-15 % efficiencies are readily available. 500 nm of molydenum is used as metal contact and 1-2 micron thick CIGS is used as absorbing material. Then 50 nm thick CdS is used as buffer layer and ZnO as window layer [3,20,32]. Typical CIGS solar cell was shown in the Figure 1.5.

One advantage of the CIGS based solar cells is, it is grown over a substrate and allow work with flexible substrates. Current techniques use vacuum co-depositon and cause higher module costs. Therefore, non-vacuum techniques are focused by many groups to reduce the cost of the CIGS based thin film solar cells. Scarcity of indium and toxicity of cadmium also causes problems for CIGS based thin film solar cells.

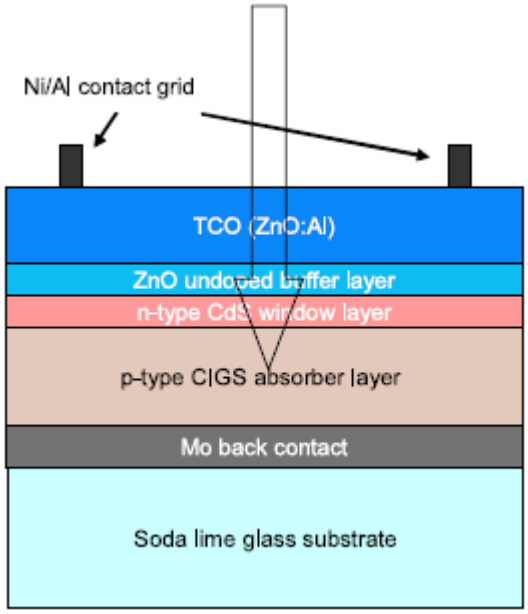

Figure 1.5 : Typical CIGS solar cell [3].

1.2.3 Dye-sensitized Solar Cells

DSC, mostly known as Gratzel cells, because of its inventor Michael Gratzel use a mesoporous titania layer covered with Ruthenium dye. The semiconductor is in contact with an ionic redox couple. High internal surface of mesoporous titania allow rapid injection of the electons from dye to the titania. Redox couple compensate for the loss electron of the dye. DSC module efficiencies up to 8 % are achieved using

the same design as research cells. Most recently, flexible DSC prepared over titanium foil are developed. Typical DSC design was given below in the Figure 1.6 [32].

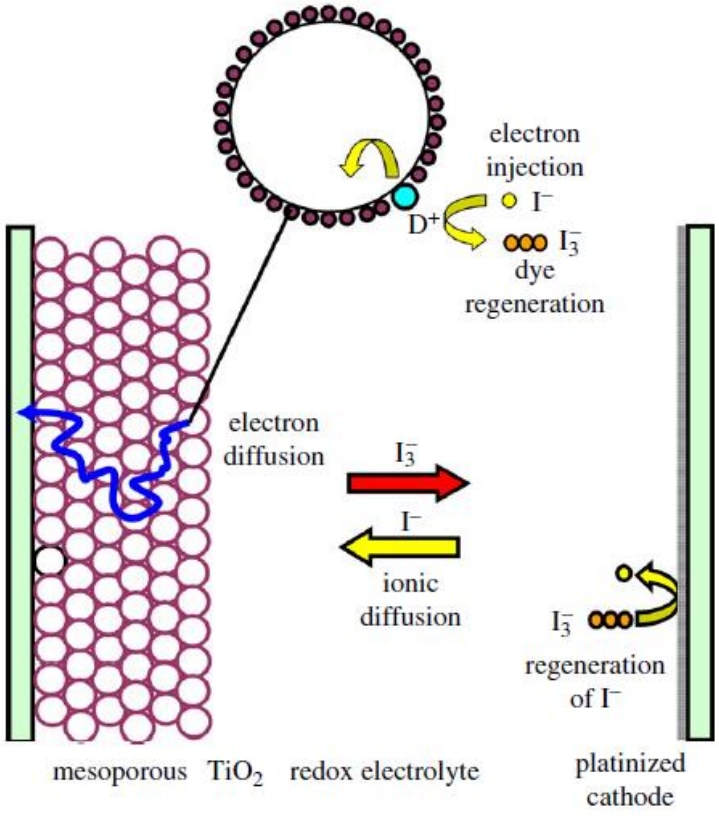

Figure 1.6 : Dye-sensitized solar cell [32].

1.2.4 Organic Photovoltaic Cells

OPV devices progress rapidly in the recent years. The cell consists of bulk heterojunction of an electron donor material such as P3HT and an electron acceptor material such as PCBM as shown in Figure 1.7. Such heterojunction is vital because of small exciton diffusion length of the polymeric substances present in the device. In the orders of few nanometers of exciton diffusion length causes complex conditions and inconsistent results because of 300 nm thick material need for the device. Layer-by-layer approaches result very low efficiency values. Despite necessity of obtaining bulk heterojunction the cost of the materials and thickness needed are promising for such solar cells. Layer of PEDOT:PSS is used to make one side selective for holes so electrons can move one side and holes another. Companies achieved up to 8 % efficiencies with test cells and research is mostly based on the identification of new materials and long-term stability [32].

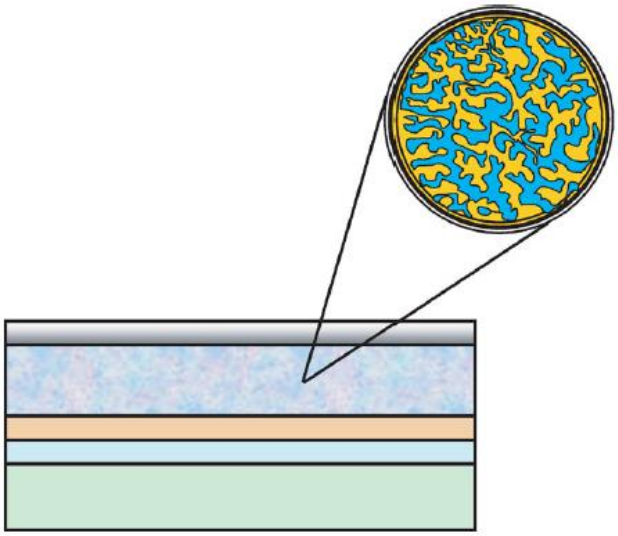

Figure 1.7 : OPV device [32].

1.3 Deposition Techniques of Copper Indium Diselenide

1.3.1 Co-evaporation

Coevaporation of CI(G)S is a process that alternates between Cu-rich and Cu-poor conditions to obtain large grains. Evaporating elemental sources to obtain CIGS film is the main focus of the coevaporation. Commercial CIGS solar panel companies also using this technique for higly efficient modules. However, because of the cosine flux distribution of the evaporation technique, sharp compositional changes or large scale uniformity is problematic. As well, top-down configuration of the sources and high application temperatures also result problems. To control composition AAS or XRF is used in the system to control and manipulate the flux of the elemental sources. Another problem is the constant supply of non-reactive Selenium in excess which causes condensation and material management problems. Despite all these problems module efficiencies more than 11 % is achieved with coeavporation of CIGS absorber layer [20].

1.3.2 Metal Selenization

Selenization of pre-deposited alloys is also used for synthesis of CI(G)S. Method is achieved with two steps. First sputtering of the metals on the surfce of the substrate is done and then these metals are converted to CIGS by annealing in selenium atmosphere. Many commercial CIGS solar panel producers also follow this

technique. These two steps mimic champion cells composition by adjusting parameters at sputtering and annelaing steps. Selenization can be done either with elemental selenium or hydrogen selenide gas. H_2Se is more reactive than elemental selenium and easy to handle. However, H_2Se is highly toxic and safety is a concern. Best module effciency achieved by this technique is 15.7 % [20].

1.3.3 Solution Processing

Solution processes are the third technique for CI(G)S preparation and vacuum is eliminated in this technique. Solution processing is also two step process in which first a layer is coated on the surface and finally layer is annealed at high temperatures to obtain large grain sized CIGS. Solution processing have many advantages as reduced capital requirements, potentially lower energy requirements and compatibility with roll-to-roll processing. Main challenge of the process is the contamination of the material by either precursor compounds or solvents. Producing dense and uniform layers is challenging [20].

Coating of the surface with CIGS and thermally annealing the material at high temperatures to increase the grain sizes is needed for final material to be used in the solar device. Module efficiencies of 11 % is achieved by solution processing techniques.

1.4 Electrodeposition of Copper Indium Diselenide

Electrodeposition of CIS was done by Jeyakumar et al. in 1994 [7]. They cathodically electrodeposited CIS films on tin oxide coated glass substrates from aqueous solutions. In their work, depostiton potential was spanned between -350 mV and -750 mV vs. Saturated Calomel Electrode (SCE). Citric acid was used in the precursor solution as a complexing agent. Sulfate salts of 5.26 mM $CuSO_4$, 18 mM $In_2(SO_4)_3$ and 3.28 mM SeO_2 were used in the aqueous solution. 5.33 mM of citric acid also added to the precursor solution. They used pH value of 1.8 for the electrodeposition experiments. They used citric acid for complexing with copper ions and bring down the deposition potential closer to the other depositing ions especially indium. By checking the thickness of the electrodeposit they found 30 minutes of deposition time is for a micron thick film. Films were characterized with XRD and tetragonal phase was found however films were polycrystalline as deposited and a

thermal annealing step is required improve the crystal quality of the film. To improve the crystal quality of the film they annealed at 425 °C in Argon atmosphere. Crystallite sizes were not calculated in the paper but FWHM values larger than 1 2θ value can be predicted from the XRD pattern given.

Vedel and coworkers also studied electrodeposition of CIS in 1994 [8]. They used the same pH value of 1.8 as Jeyakumar did and as well 2.45 pH value with H_2SO_4 was also tried without using citric acid in the precursor solution. They referred the potentials as Mercury Sulfate Electrode (MSE) and potentials below than -0.9 V suitable for electrodeposition of CIS.

In 1997 Tzvetkova and coworkers used thiocyanate as a comlexing agent for the electrodeposition of CIS [9]. In this work, they used molybdenum coated glass substrates as work electrodes. CuCl, $In_2(SO_4)_3$ and SeO_2 with a total concentration of 8.5 mM but in different ratios used as precursor solution. By adding acetate buffer to the deposition solution, they fixed pH at 5. They found 1 V vs. SCE suitable for electrodeposition of CIS. XRD data of the as-deposited samples, which was given below in Figure 1.8, show weak polycrystalline properties because of broad reflections from the characteristic tetragonal CIS peaks. To improve crystalline properties they annealed the samples either argon atmosphere or selenium atmosphere.

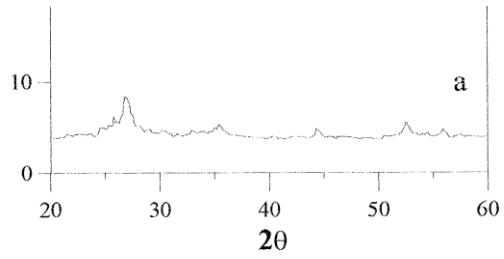

Figure 1.8 : XRD data of the as deposited film [9].

In 2000, Kemell and coworkers electrodeposited CIS the same way as Tzvetkova did by using thiocyanate as complexing agent [10]. However, they used more acidic condition (pH 2.7-3.1) for electrodeposition. They used 100 nm molybdenum sputtered glass samples as work electrodes and Pt plate as counter electrode. They kept CuCl and SeO_2 concentrations constant as 0.05 M and 0.001 M respectively. They spanned $InCl_3$ concentraiton from 0.02 M to 0.125 M. They used 4 M KSCN as complexing agent and dilute HCl to adjust pH. They found the film composition

independent of the Cu/In ratio and speculated CIS formation proceeds via $Cu_{2-x}Se$ formation. They analyzed the films by XRD and found amorphous as deposited. They also needed an annealing step under argon atmosphere to increase the crystal quality of the film electrodeposited.

In 2001, Dharmadasa and coworkers electrodeposited CIS films on Titanium substrates at room temperature [11]. Salt concentrations of 0.005 M $CuCl_2$, 0.005 M $InCl_3$ and 0.001 M SeO_2 were used in the precursor solution. They adjusted pH at 1.5 with dilute HCl. They stirred the electrodeposition solution in the experiment. As deposited films were polycrystalline because of broad and weak reflections of characteristic tetragonal chalcopyrite structure of CIS as shown in Figure 1.9. Annealing of the films to improve crystal quality of the films was also studied by the group. From XRF measurements, they ended with possibility of the occurrence of more than one phase because of the high content of Cu and Se. Both possible compounds of CIS and Cu_2Se give rise to the same peaks.

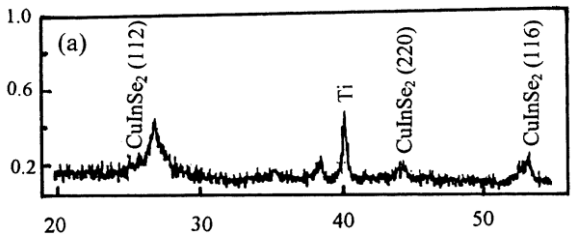

Figure 1.9 : XRD data of the as deposited film [11].

In 2009, Benouttas and coworkers electrodeposited CIS on Mo substrates using thiocyante as a complexing agent [19]. In electrolyte solution, they used 1 mM CuCl, 5 mM $InCl_3$, 1 mM SeO_2 and 3.5 M KSCN. They fixed pH at 4 and spanned the temperature of the electrodeposition solution from 20 °C to 80 °C. However, increase of the temperature increased the Cu content of the film. As deposited films showed poor crystallinity and had small grains. SEM images of the films were given below in Figure 1.10.

In 2009, Gujar and coworkers electrodeposited CIS from 10 mM $CuSO_4$, 10 mM SeO_2 and 10 mM $In_2(SO_4)_3$ precursor solution [12]. By using dilute sulfuric acid they adjusted pH of the solution between 1.5-2.0 range. They used indium tin oxide, fluorine-doperd tin oxide, nickel, molybdenum and stainless steel substrates. Depositon potential range of -600 mV to -1000 mV vs Ag/AgCl reference electrode

was applied without stirring the solution. They found -700 mV as best condition for high crystallinity and composition.

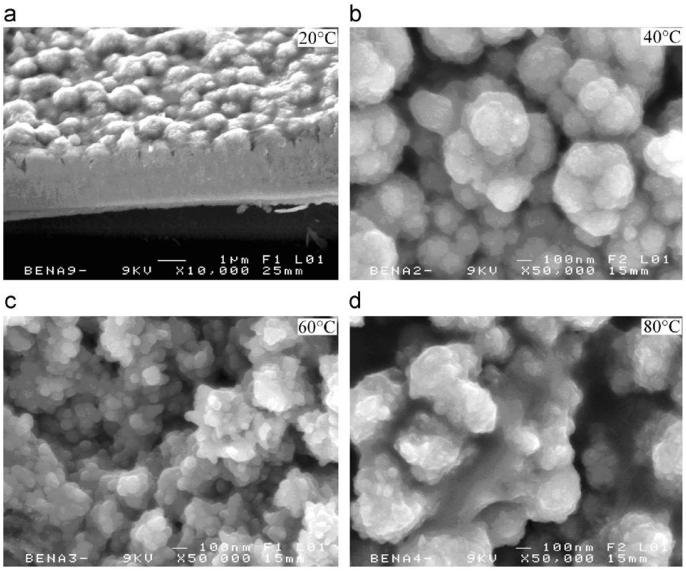

Figure 1.10 : SEM images of the films prepared at different temperatures [19].

Despite claiming no secondary phases present in the deposited film it is clear from the XRD results, which were given in Figure 1.11, a shoulder corresponding to either $Cu_{2-x}Se$ or In_2Se_3 phase predicted by other research groups is present. As well, they predict the crystallite size of the samples around 60 nm but again an estimation of FWHM value from XRD results gives less than 10 nm of crystallite sizes.

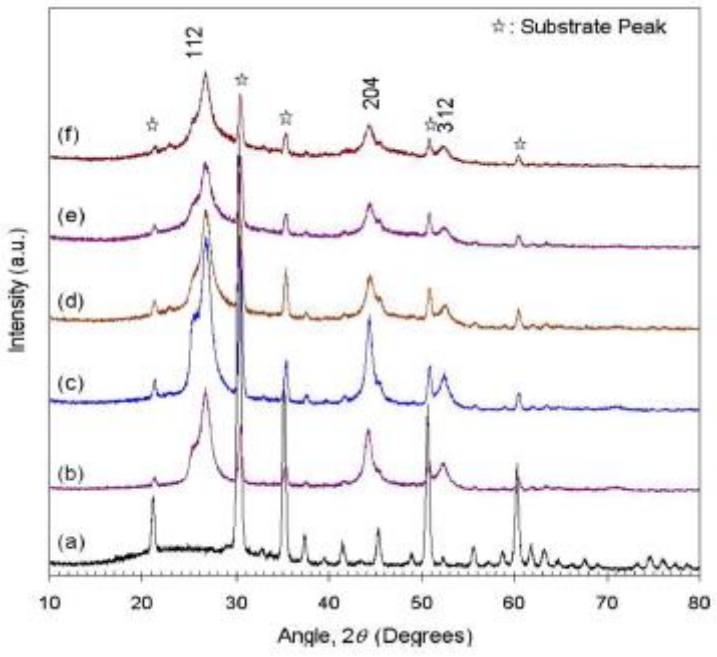

Figure 1.11 : XRD data of the as deposited films [12].

In 2010, Lincot and coworkers studied electrocrystallization mechanism of CIS [13]. They used 1 mM $CuSO_4$, 1.7 mM SeO_2 and 6 mM $In_2(SO_4)_3$ as precursor solution. They adjusted pH at 2 and used supporting electrolyte. They found at low overpotential values no indium deposition was observed.

Sanz and coworkers in 2010, found pulsed electrodeposition of CIS enhances microstructure of the CIS film [24]. They carried electrodepositon on ITO samples. Two different deposition concentration and three different pulse durations evaluated in the paper. pH of the solution was adjusted with dilute sulfuric acid in the range of 2.10-2.70 values. All precursor solutions kept constant and 2 mM for each for high concentration precursor solution and 0.3 mM for each for low precursor solution. However, electrodeposited films given in the Figure 1.12 below showed poor crystallinity with broad and weak reflections. The films obtained had more uniform grain sizes with pulse technique. They predicted the film uniformity and improvement on the film morphology because of more controlled diffuse regimes under control of the pulse durations.

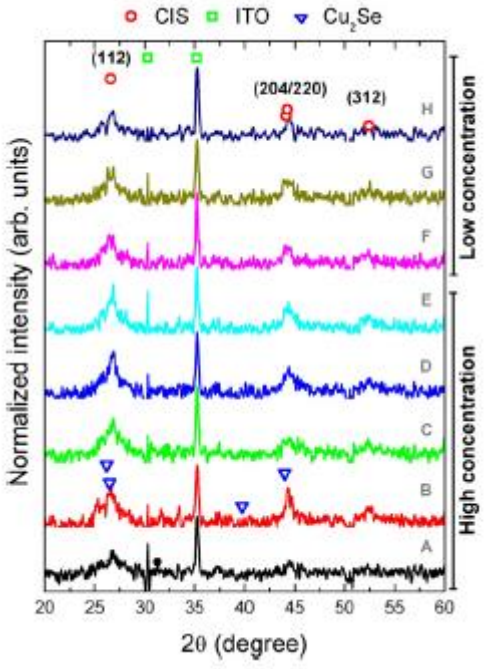

Figure 1.12 : XRD data of the as deposited films [24].

In 2011, Li and coworkers electrodeposited CIS films and worked on their microstructures [14]. They found the Se/Cu ratio plays an important role on the composition and microstructure of the film. They advise high concentrations of Cu and In for high crystallinity and large grain sized chalcopyrite phase. They used 1.28-

1.92 mM SeO_2, 1.00-1.15 mM $CuSO_4$ and 0.8-3 mM $In_2(SO_4)_3$ in the precursor solution. They adjusted pH at 1.8 by dilute sulfuric acid solution. 0.3 M K_2SO_4 was used as supporting electrolyte. The applied potential was 0.95 V vs. MSE. They proposed a deposition mechanism for CIS as shown in the Figure 1.13. Small grain sized films were obtained with Cu-poor conditions and large grain sized obtained for Cu-rich conditions. As well they concluded $Cu_{2-x}Se$ formation for large grain size CIS film formation.

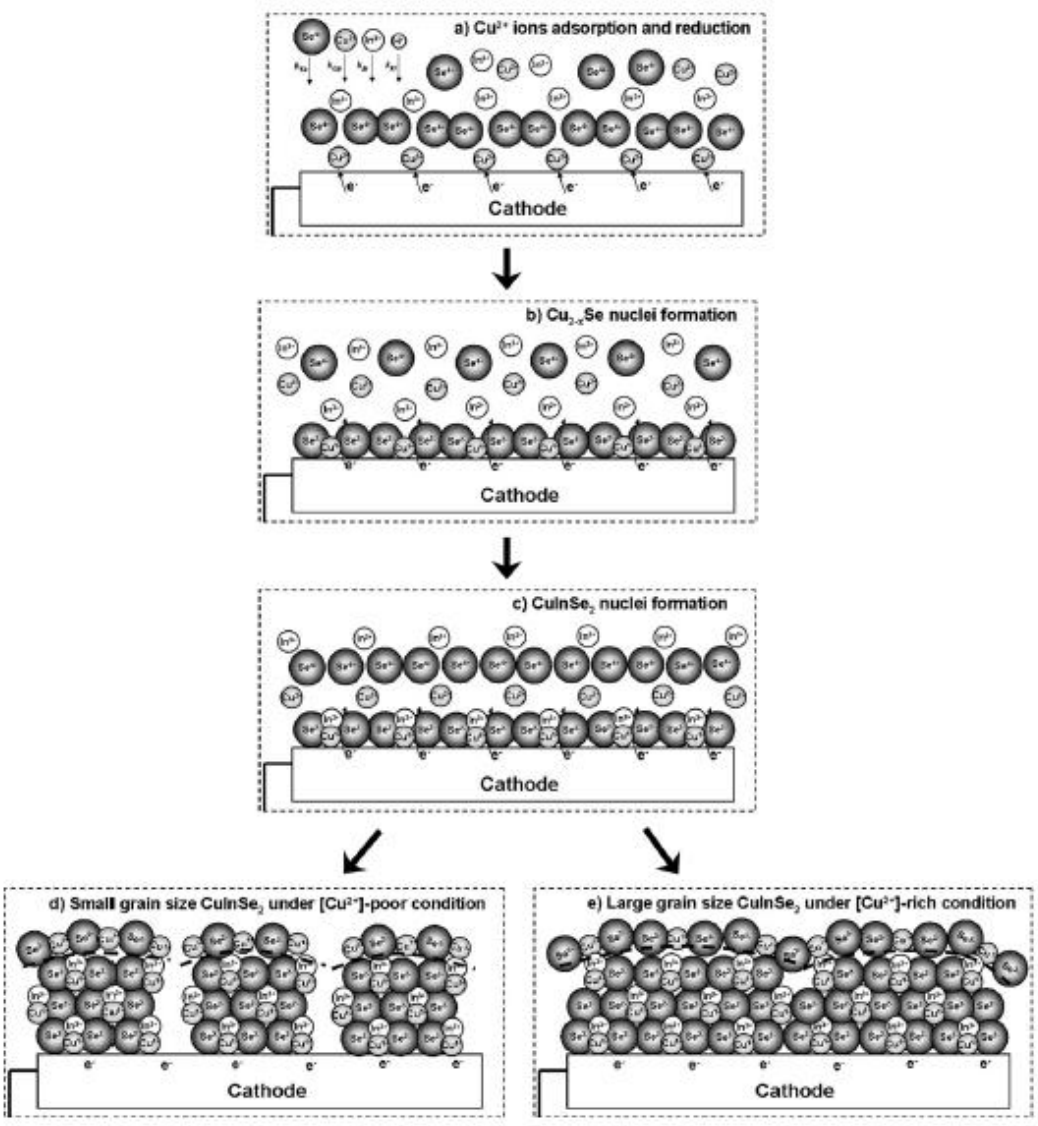

Figure 1.13 : Deposition mechanism of CIS films [14].

In 2012, Mallouk electrodeposited CIS nanowires in the pores of anodic aluminum oxide templates [18]. They found as deposited wires consist of 2 nm crystallite sizes and crystallinity improved up to 40 nm upon annealing. XRD data of the deposited films were given below in Figure 1.14.

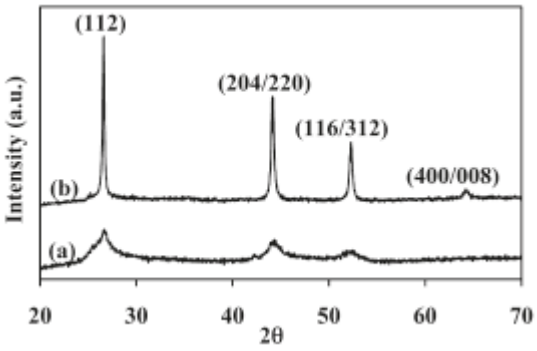

Figure 1.14 : XRD data of the as deposited and annealed films [18].

In 2013, Lin and coworkers studied the effect of supporting electrolyte on the crystal quality of the electrodeposited CIS film [16]. They found the concentration of the supporting electrolyte enhances the crystal quality of the film but excess of the supporting electrolyte causes formation of aggregates and decreases the crystal quality of the film. Good quality films also achieved without addition of supporting electrolyte. XRD results were given below in the Figure 1.15.

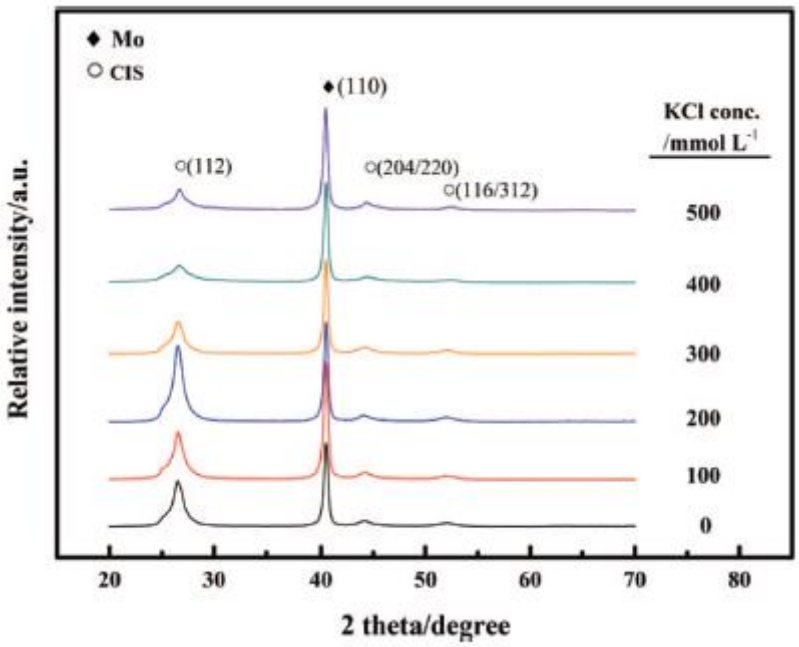

Figure 1.15 : XRD data of supporting electrolyte experiments [16].

2. EXPERIMENTAL

2.1 Materials

All chemicals used in the reaction are analytical grade. $InCl_3$ (%99.99) was supplied from Alfa Aesar. SeO_2 was supplied from Merck. $CuCl_2.2H_2O$ was supplied from Riedel. HCl %36,5 was supplied from Sigma Aldrich. MilliQ pure water (18.2 mΩ) was used in the electrochemical synthesis.

2.2 Electrodeposition

2.2.1 Optimization of the Deposition Potential

Electrodeposition of CIS was done on Commercial Molybdenum coated glass layers having sheet resistance of 0.55 Ω/sq with a Gamry 600 potentiostat. Deposition area was 1.5x1.5 cm^2, which was larger than typical values in the literature. Before electrodeposition all samples were cleaned with deionized water, acetone and deionized water again.

Electrochemical cell was a three-electrode cell consisting of Pt wire as an auxiliary electrode, Ag/AgCl as a reference electrode and Molybdenum coated glass layers as work electrode. Deposition was done at room temperature with potentiostatic pulse method with 0.1 s on and 0.1 s off time without stirring the solution. Deposition time was chosen as 30 minutes. Deposition was done without stirring the solution.

Initial concentrations of 1 mM $CuCl_2$, 1.7 mM SeO_2, 6 mM $InCl_3$ and 0.2 M HCl were chosen as starting point for all parameter optimizations. To investigate parameters individually, first spanning the deposition potential was chosen. In literature, for electrodeposition of CIS very large potential range was applied. As a start point, -0.5 V vs. Ag/AgCl reference electrode was tried because this voltage was mentioned in many papers. Potential was decreased down to -0.65 V by checking every 25 mV values.

2.2.2 Investigation of the Precursor Concentrations

Concentrations of $CuCl_2$, SeO_2 and $InCl_3$ were spanned by checking higher and lower values of starting parameters. Concentration of salt precursors was varied for $CuCl_2$ from 1 mM to 1.5 mM, for SeO_2 from 1mM to 1.7 mM and for $InCl_3$ from 4.5 mM to 7.5 mM. HCl was used to increase the acidity of the solution and changed from 0.01 M (pH 2.16) to 0.2 M (pH 1.09).

2.3 Characterization of CIS films

All deposits were checked with XRD for crystallinity and phase analysis. Rigaku Miniflex 600 diffractometer with Cu Kα (1.542 Å) radiation was used as equipment. Operation conditions were set as 40 kV and 15 mA. Analysis parameters were chosen as 3-80° 2θ measurement range, 0.02° for step size and 1°/min. Crystallite sizes were calculated from Debye Scherrer equation with full width at half maximum (FWHM) values of (112) CIS peak located at 26.6° 2θ. The morphology and composition of the deposits was investigated by using a JEOL JSM-6510LV scanning electron microscope with EDS attached. Optical microscope images were taken by a Nikon LV100POL optical microscope with digital camera. AFM measurements were done with Nanosurf Easyscan equipment. FTIR measurements were done with Perkin Elmer FTIR-ATR reflectance spectrometer.

3. RESULTS AND DISCUSSION

Deposition parameters were adapted from Lincot et al. [13] but pulsed electrodeposition technique and more acidic media was used. Se(1.7 mM)/Cu(1 mM) ratio of 1.7 and 6 mM of $InCl_3$ was chosen as start point. Electrodeposition potential was spanned between -500 mV to -650 mV. XRD results were given below in Figure 3.1. Voltage range of -525-575 mV gave highest intensities and therefore deposition potential of -550 mV was chosen for further optimizations.

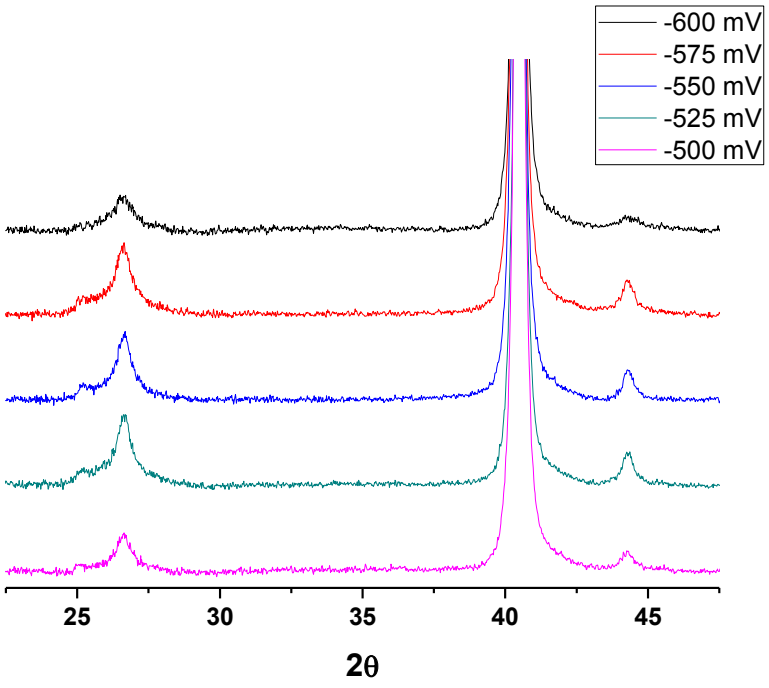

Figure 3.1 : XRD data of potential optimization.

Then, concentrations were spanned separately. Decreasing Se/Cu ratio by increasing copper concentration or decreasing selenium concentration from 1.7 to 1.36 and 1.27 respectively increased the intensity of an extra peak located at 25.2° 2θ as shown in Figure 3.2. This peak was also seen by many groups as a shoulder to peak at 26.6° 2θ and speculated as In_2Se_3 phase [33-34]. However, missing of several reflections especially at 12.6° 2θ made this assignment unclear [33].

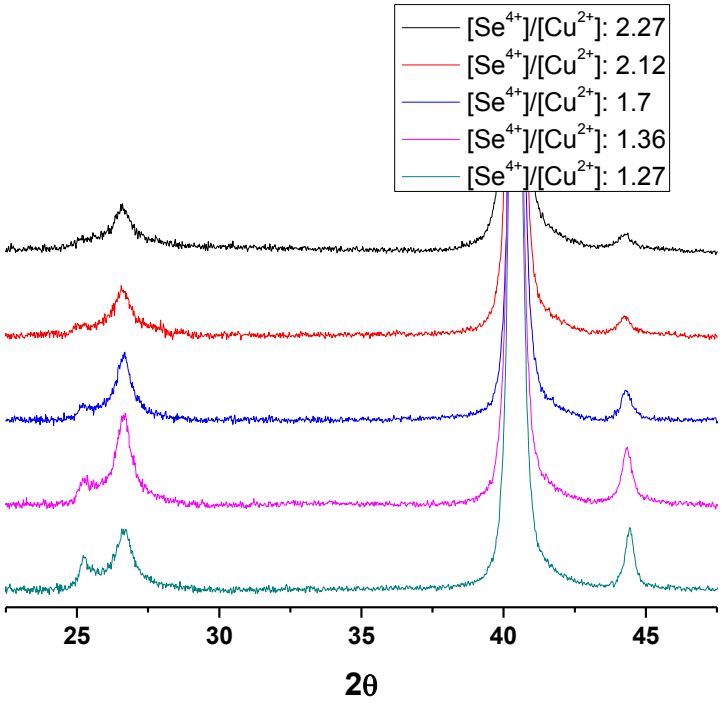

Figure 3.2 : XRD data of Se/Cu ratio experiments.

Increasing Se/Cu ratio either by increasing selenium concentration or decreasing copper concentration to 2.12 or 2.27 respectively decreased the intensity of the characteristic peaks of CIS. In the Figure 3.3, ratio of (112)/(204)(220) peaks are plotted with respect to Se/Cu ratio. Se/Cu ratio is directly proportional to the ratio of (112)/(204)(220) planes and (204)(220) planes are more oriented for low Se/Cu ratios.

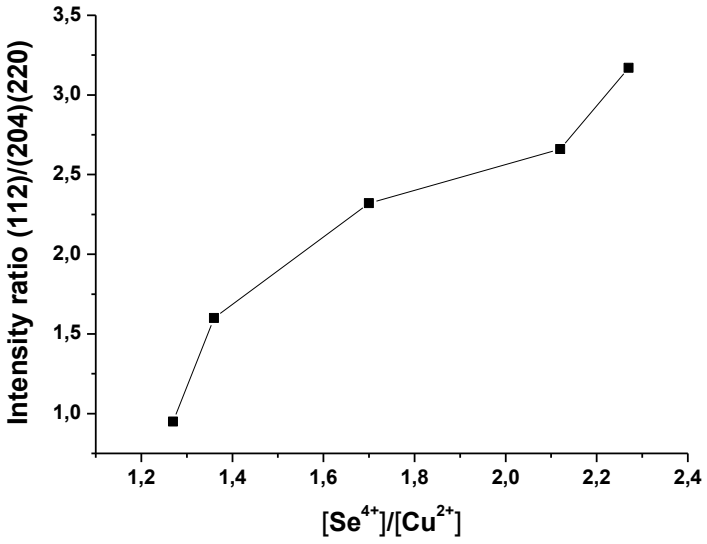

Figure 3.3 : Intensity ratio of (112)/(204)(220) peaks wrt. Se/Cu ratio.

To understand these changes Se/Cu ratio further decreased to 1.02 and 0.67 by changing both copper and selenium concentrations at the same time and results are shown in the Figure 3.4 below. In addition to the peak located at 25.2° 2θ another peak evolved at 28.5° 2θ. XRD analysis from database matched these peaks including peak located at 26.6° 2θ as wurtzite $CuInSe_2$ ((100),(002),(101), pdf card no: 1-78-5190) found by Brutchey et al [35]. This metastable phase was assigned for the first time for electrochemical deposition.

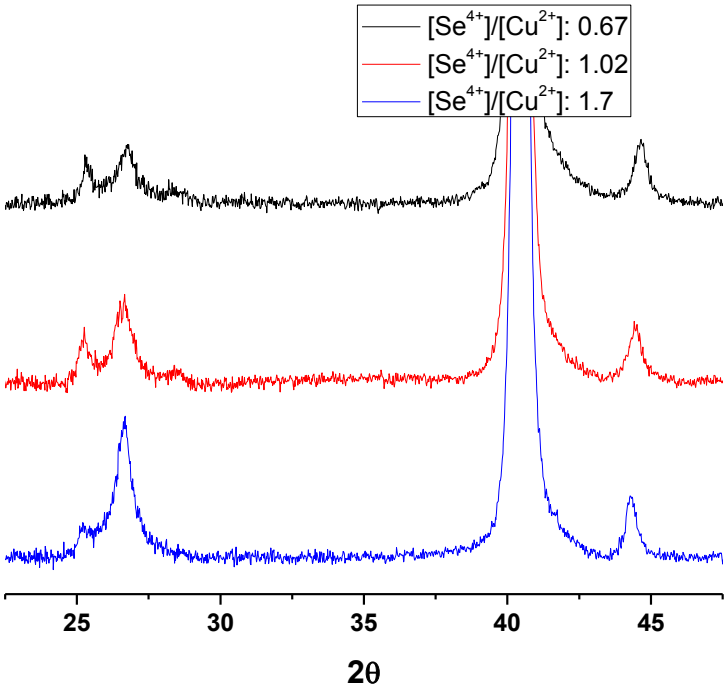

Figure 3.4 : XRD data of low Se/Cu ratio experiments.

We believe deposition of CIS occurs with a competition between tetragonal phase with Cu-rich nature because of Cu_2Se lattice match and wurtzite phase with In-rich nature because of In_2Se_3 lattice match. In Figure 3.5, ratio of these two phases are given with higher values of wurtzite phase for low Se/Cu ratios.

Change of indium concentration between 7.5 mM and 4.5 mM did not affect the intensities much with 6 mM resulting the highest intensities as shown in Figure 3.6.

The acidity of the solution was changed to investigate pH effect on crystallite sizes. HCl concentration is changed from 0.01 M (typical literature values: pH 1.5-4.0) to 0.2 M. Increasing the acidity of the solution enhanced the crystallization of the deposit as shown in the Figure 3.7 with decreasing FWHM values of the characteristic (112) peak of CIS.

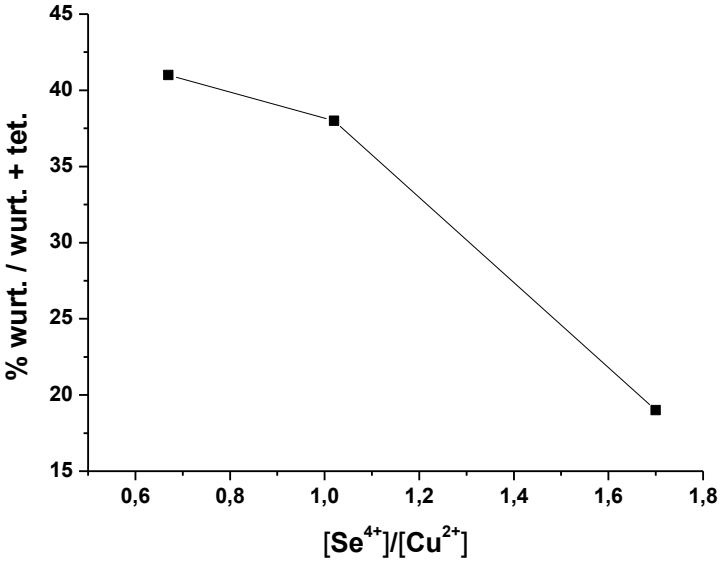

Figure 3.5 : % wurtzite ratio wrt. Se/Cu ratio.

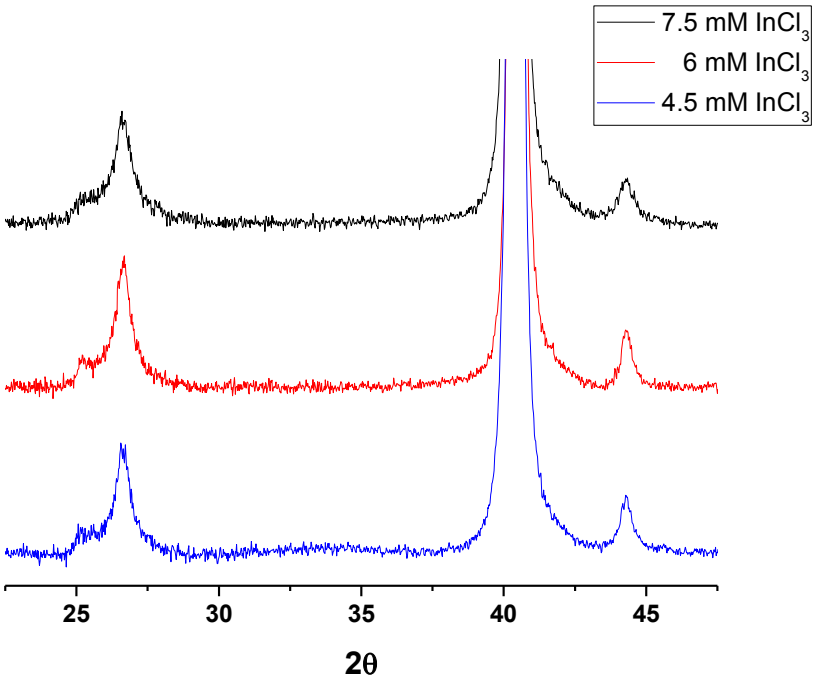

Figure 3.6 : XRD data of Indium concentration experiments.

Crystallite sizes were calculated based on Debye-Scherrer equation and given in the figure below. Crystallite sizes increased from 7.57 nm (FWHM: 1.44° 2θ) for 0.01 M HCl (pH 2.16), which is similar as common results of literature which have 1.5-3° 2θ FWHM values [10,11,16,18,19], to 10.10 nm (FWHM: 1.08° 2θ) for 0.05 M HCl (pH 1.58) and to 17.31 nm (FWHM: 0.63° 2θ) for 0.2 M HCl (pH 1.09).

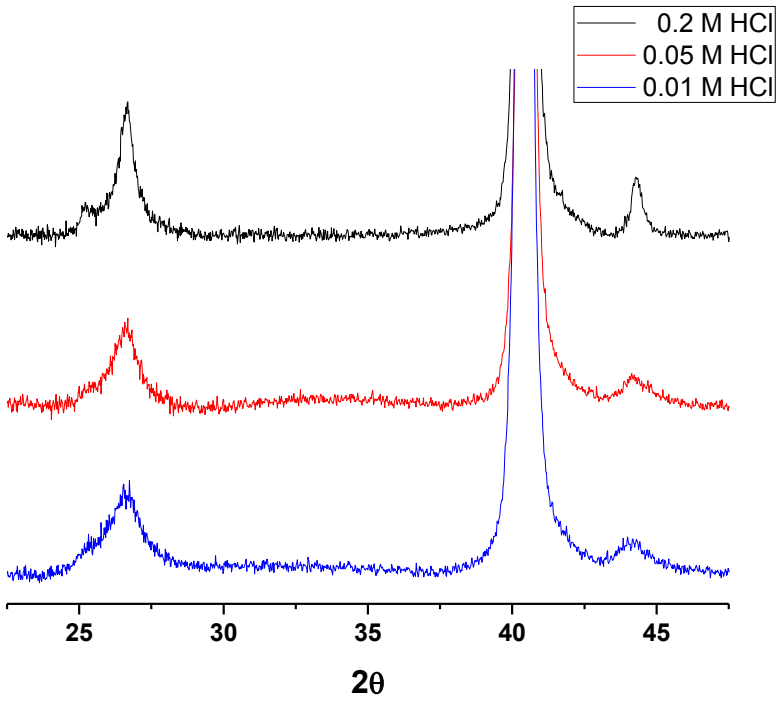

Figure 3.7 : XRD data of acidity experiments.

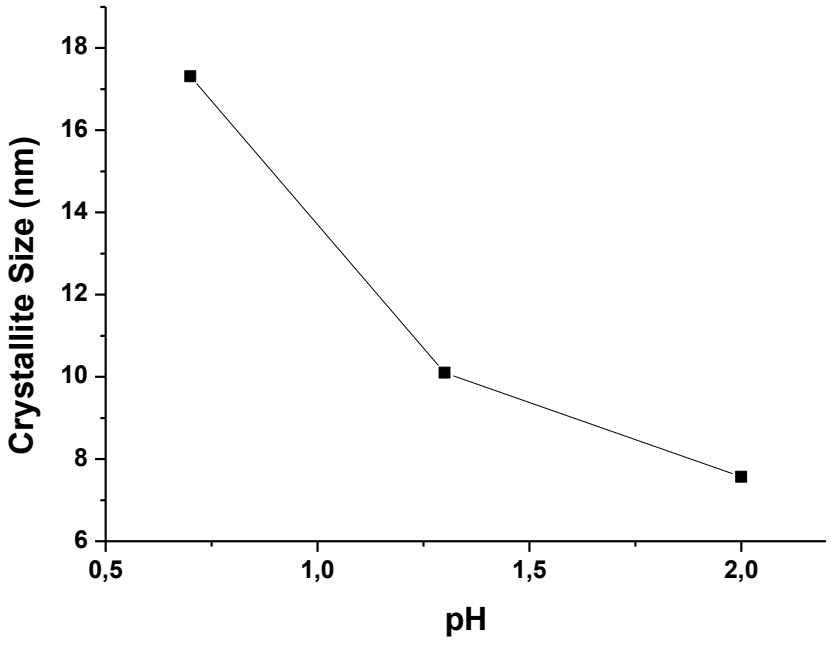

Figure 3.8 : Crystallite sizes wrt. acidity of the solution.

Further increase in the acidity of the solution caused peeling off the deposited film from the surface at electrodeposition step or at washing step because of low roughness value of the commercial Mo substrates.

Pulse duration was also checked by changing on-off time from 100 ms to 50 ms and to 20 ms. XRD analysis of the pulse experiments did not show any considerable change with resulting best values for 100 ms on and 100 ms off time as shown in Figure 3.9 below. However, optical microscope images of the deposits show a trend for smaller aggregates for short pulse durations.

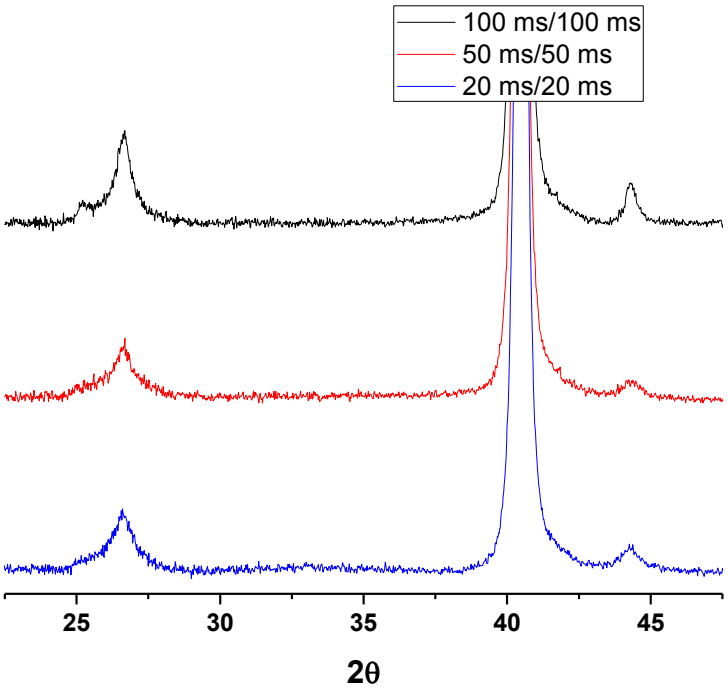

Figure 3.9 : XRD data of pulse duration experiments.

Optical microscope images in Figure 3.10 and Figure 3.11 below, indicate two types of growth one smooth and one with aggregates. In literature, this aggregate phase was observed mainly with mentioned as dendritic type growth [12,15,19,24,25,26]. Wurtzite phase dominant samples have much larger portion of smooth type deposit. Aggregate deposits were increased with diminishing wurtzite phase peaks.

Optical microscope images of low Se/Cu ratio samples consist of smaller aggregates. Especially 0.67 Se/Cu ratio sample have more uniform and smaller aggregates on. SEM images of these samples were given in the Figure 3.12 for 1.02 Se/Cu ratio sample and in the Figure 3.13 for 0.67 Se/Cu ratio sample.

Scanning electron microscope images also confirm smooth-aggregate situation as shown in the Figure 3.14 below. Wurtzite phase dominant 1.27 Se/Cu ratio sample have smoother surface, with less portion of aggregates over, than Se/Cu ratio of 1.7 sample.

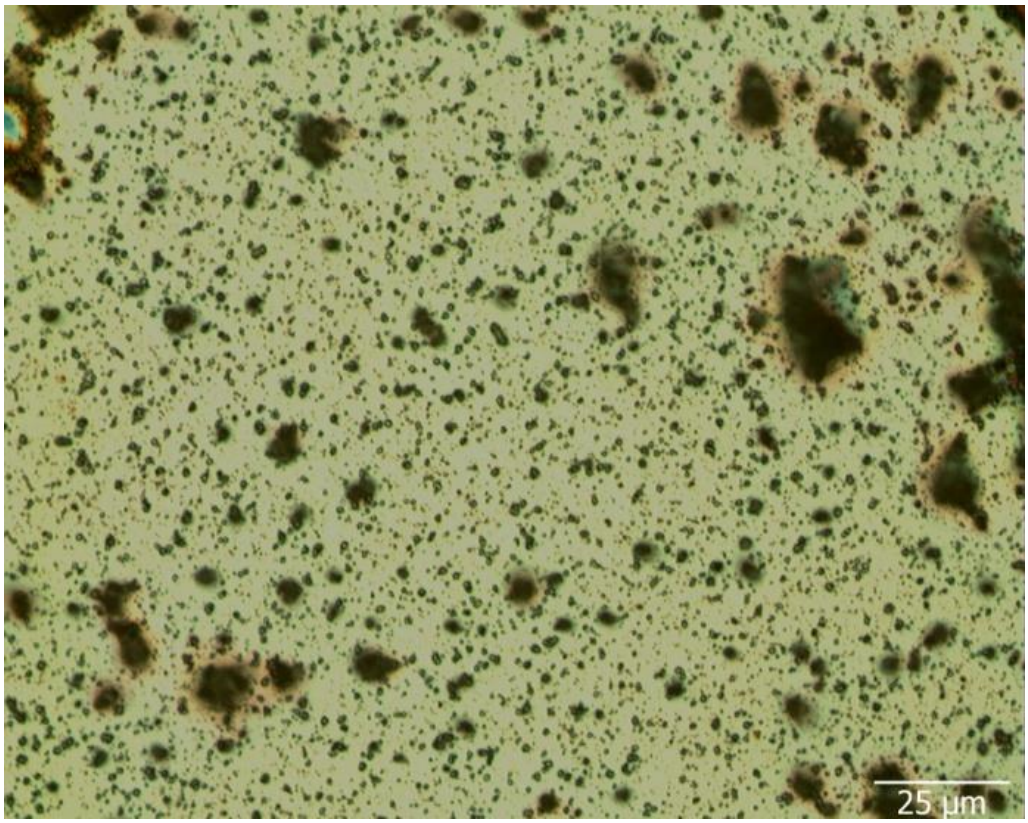

Figure 3.10 : Optical Microscope images of smoooth structures.

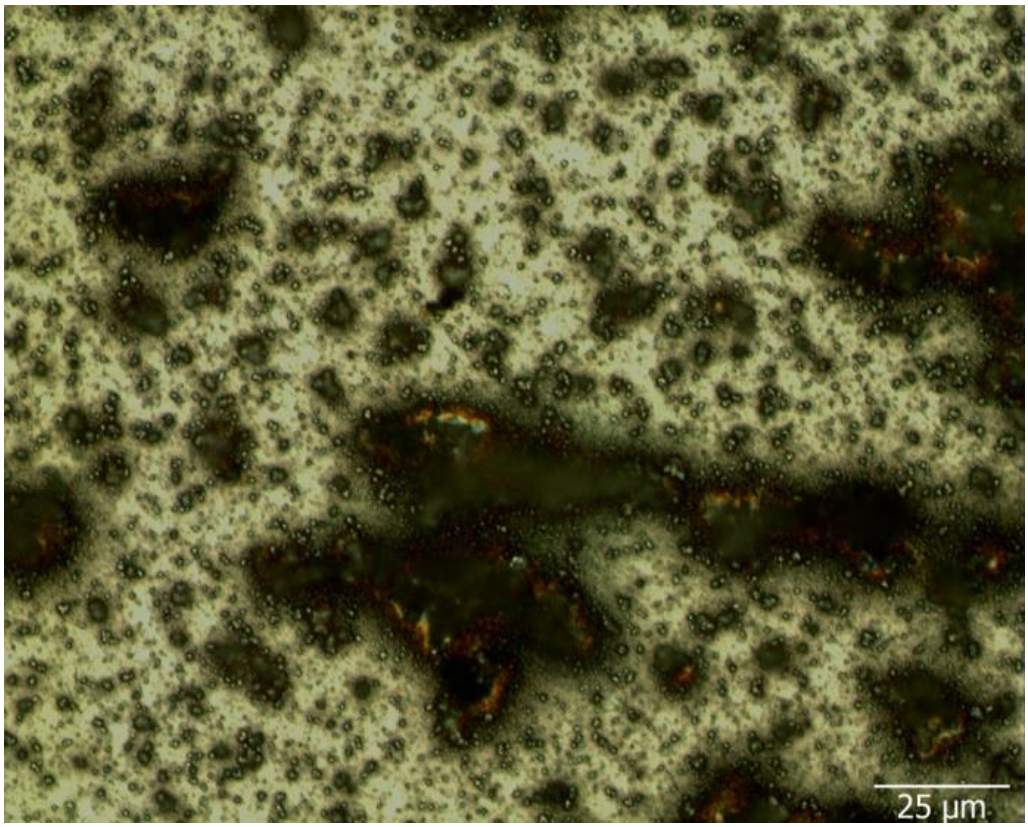

Figure 3.11 : Optical Microscope images of aggregate structures.

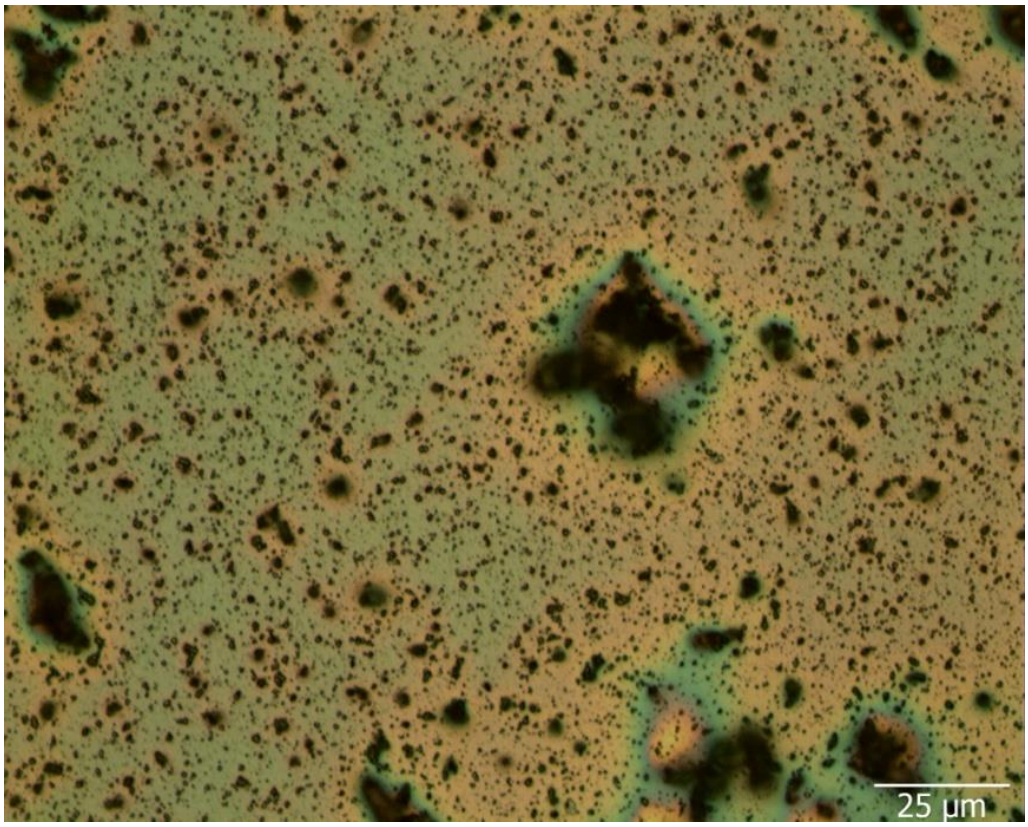

Figure 3.12 : Optical imges of 1.02 Se/Cu ratio sample.

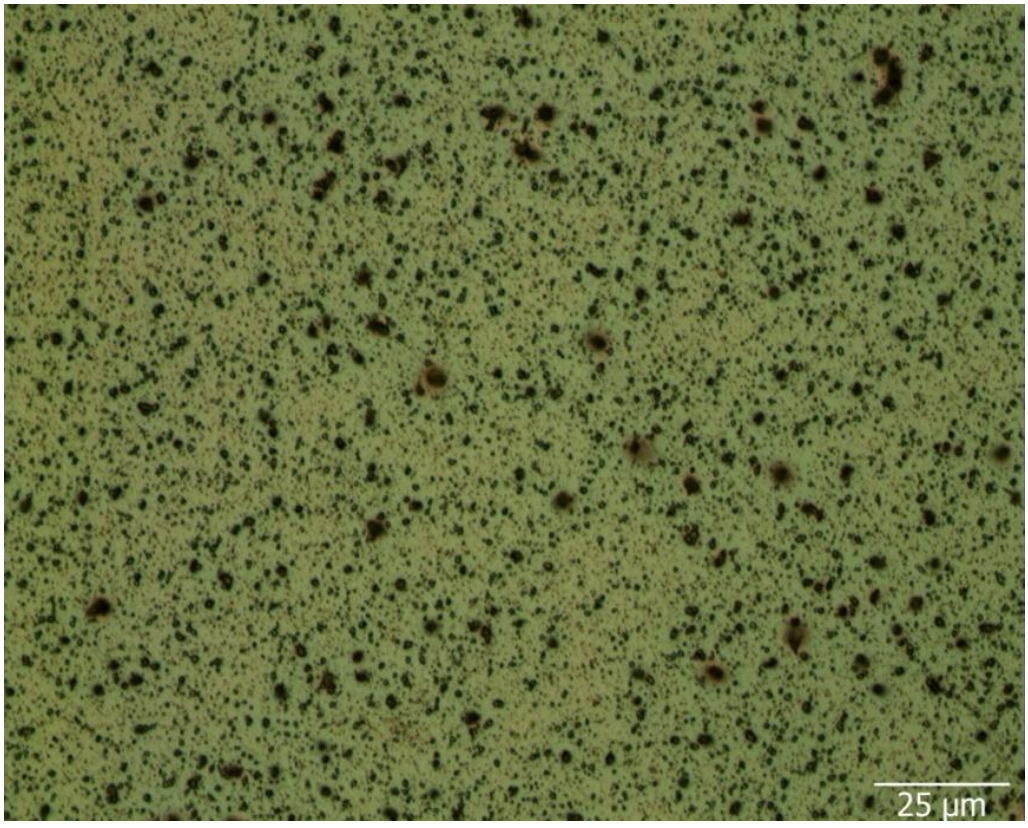

Figure 3.13 : Optical imges of 0.67 Se/Cu ratio sample.

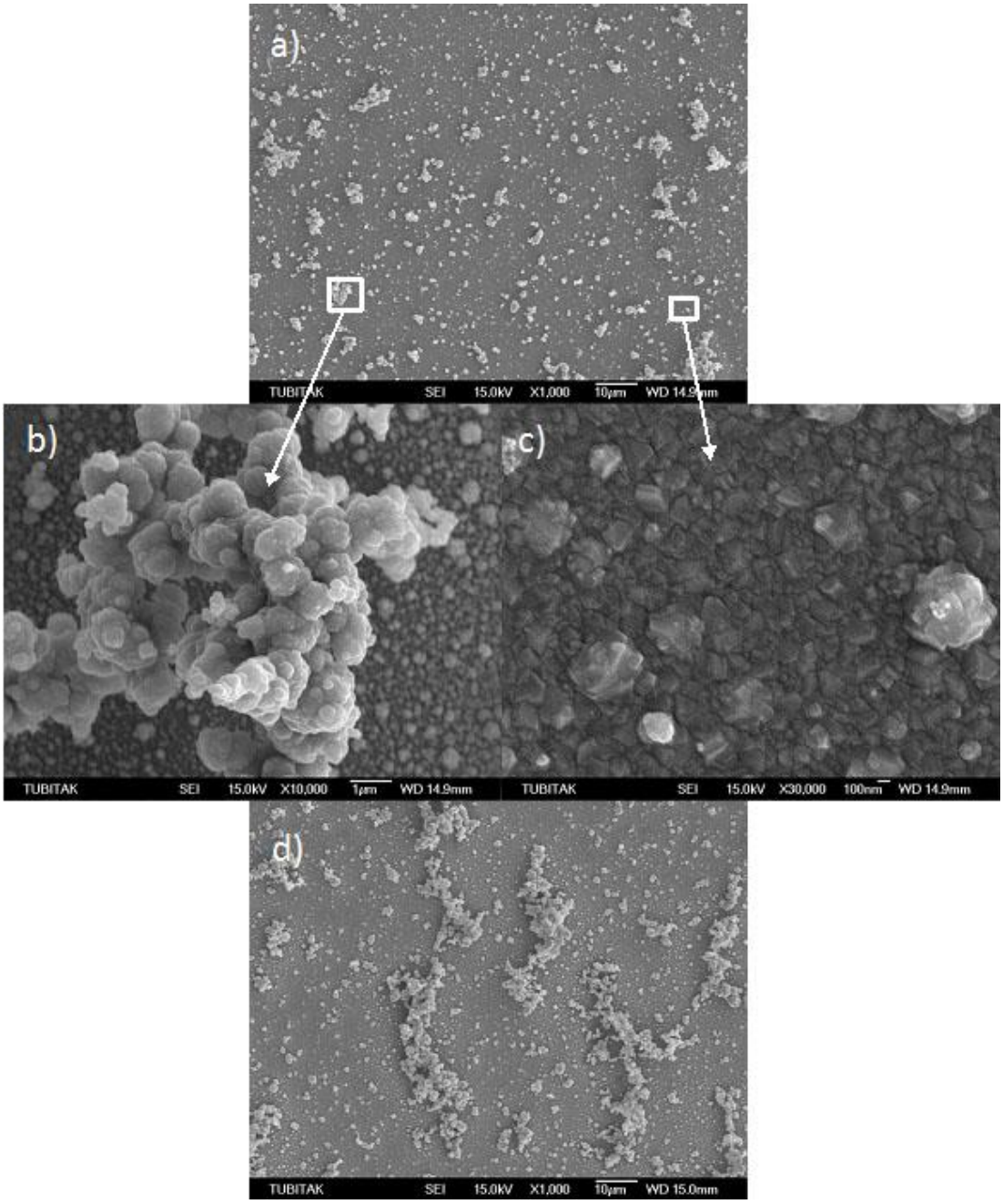

Figure 3.14 : SEM images of a) smooth structures, b) magnified aggregates of a, c) magnified smoooth part of a and d) aggregate structures.

Energy dispersive X-ray spectroscopy (EDS) analysis gave $Cu_{1.30}In_{0.75}Se_{1.94}$ for smooth surfaces of 1.27 Se/Cu ratio deposit which is consistent with wurtzite phase of $Cu_{1.32}In_{0.94}Se_{2.00}$ given by Brutchey et al. Se/Cu ratio of 1.7 deposit gave $Cu_{1.09}In_{0.83}Se_{2.08}$ atomic ratios consistent with increased selenium concentration also increased selenium amount at the deposit [35]. Aggregate type structures were more copper rich with $Cu_{1.45}In_{0.55}Se_{2.00}$ atomic ratios. Cu-rich nature of these aggregates

may be influenced by the higher tendency of Cu-Se phases present with tetragonal growth as lattices match.

An FTIR measurement of the material was shown in the Figure 3.15 below. Peak at 472 cm^{-1} corresponds to the metal-selenium bonds of the CIS.

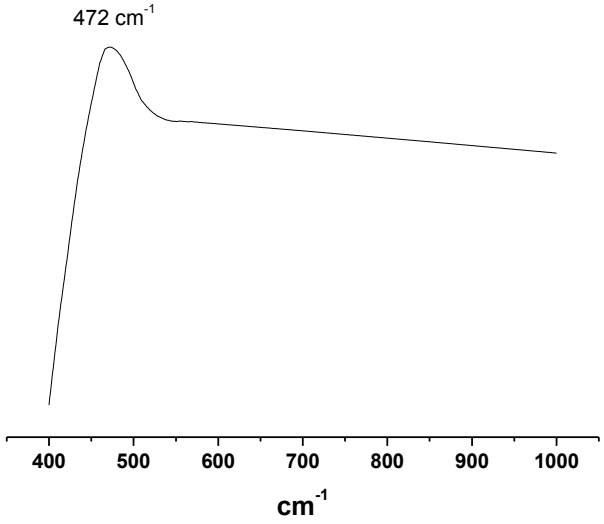

Figure 3.15 : FTIR spectrum of CIS.

By using AFM technique, suface analysis of commercial molybdenum coated glass substrates were done and surface roughness was measured. AFM results for commercial substrates are given in the Figure 3.16 below.

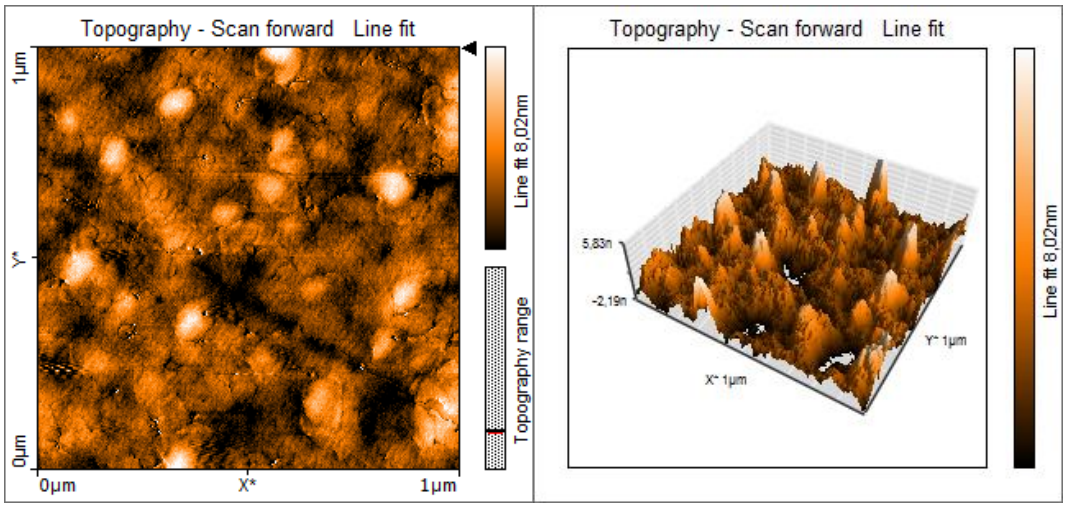

Figure 3.16 : AFM topography of commercial Mo coated glass substrate.

Sample used for high acidity experiments in which CIS layer did not peel off from the surface was also checked with AFM and results are given in the Figure 3.17

below. Surface roughness of the commerical substrates was 0.94 nm but evaporated samples created for the experiments was 3.87 nm. This four-fold surface roughness difference accounts for the stickness of the deposit on the surface.

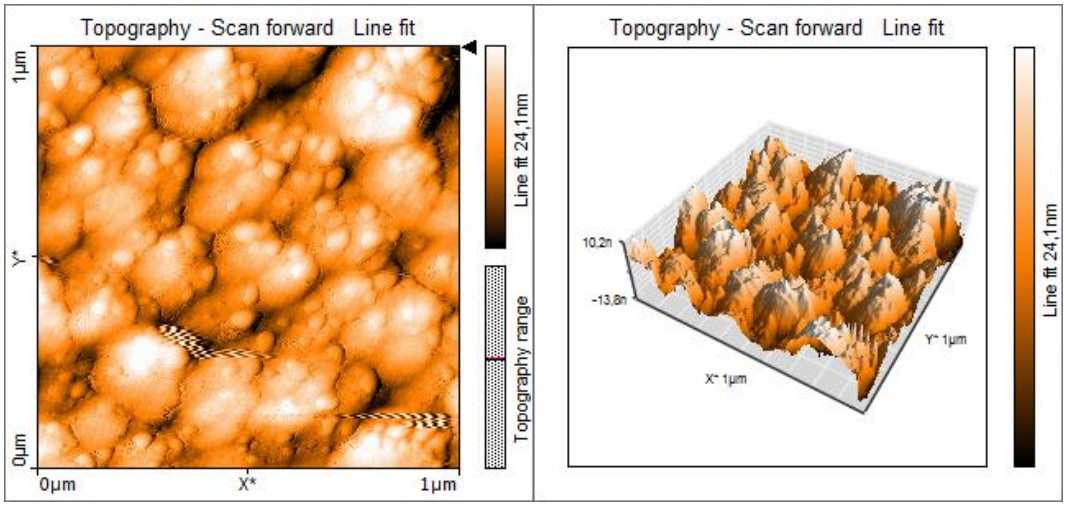

Figure 3.17 : AFM topography of Mo evaporated glass substrate.

After understanding the surface topology of the substrates, electrodeposited samples was checked to understand the difference between the aggregate and smooth surfaces. Se/Cu ratio of 1.7 sample in which more aggregate phase present and small wurtzite peak present, have surface roughness value 18.5 nm. AFM results of this sample was given below in Figure 3.18.

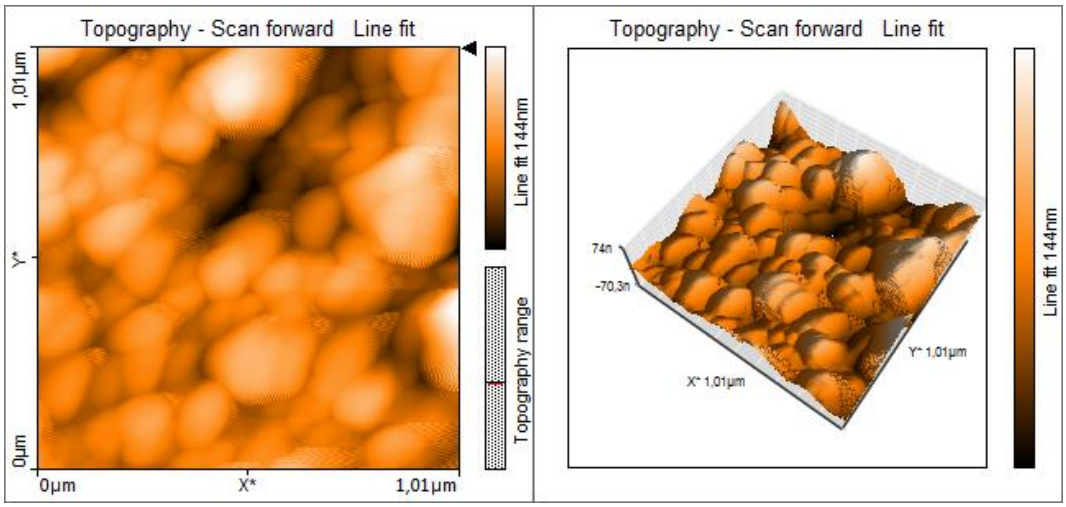

Figure 3.18 : AFM topography of Se/Cu ratio of 1.7 sample.

However, Se/Cu ratio of 1.27 sample which was smoother and wurtzite peak was more obvious, had surface roughness value of 13.03 nm. AFM results of this sample was given below in Figure 3.19.

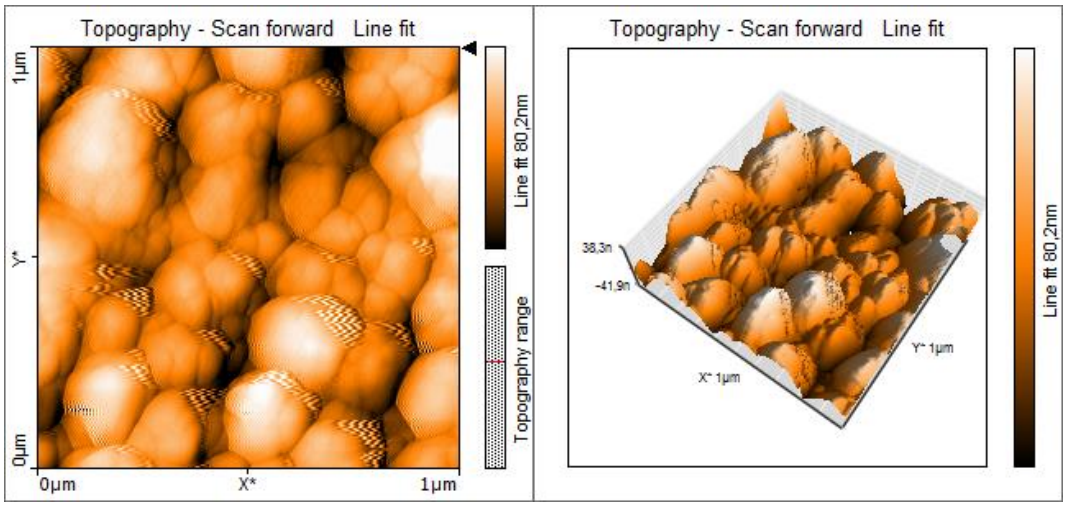

Figure 3.19 : AFM topography of Se/Cu ratio of 1.27 sample.

As well, Se/Cu ratio of 1.36 sample had surface roughness value of 13.77 nm which is more than but close to 1.27 Se/Cu ratio sample. AFM results of this sample was given in Figure 3.20. These both samples were shown less rougher than the 1.7 Se/Cu sample. This result also support SEM and optical microscope results.

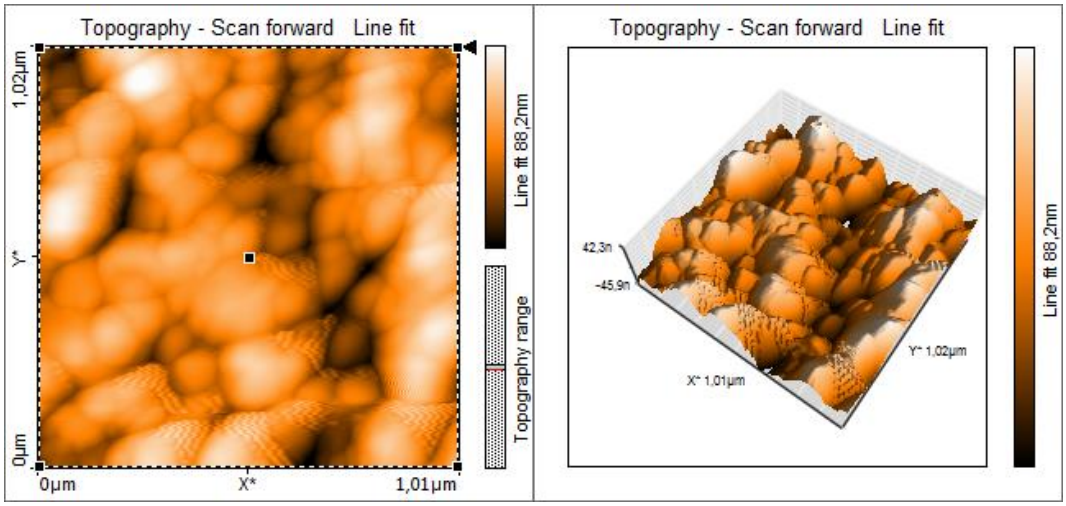

Figure 3.20 : AFM topography of Se/Cu ratio of 1.36 sample.

Electrochemical impedance measurements were done in 0.1 M NaClO4/H2O solution between 10 mHz - 100 kHz frequency range. Ag wire was used as reference electrode, Pt wire was used as counter electrode and electrodeposited CIS samples were used as work electrodes. Electrochemical impedance measurement results were shown in Figure 3.21, Figure 3.22, Figure 3.23 and Figure 3.24 below.

Bode phase and magnitude results give higher values for 0.2 M sample. These results show higher resistive characteristics for 0.2 M sample which may be caused because

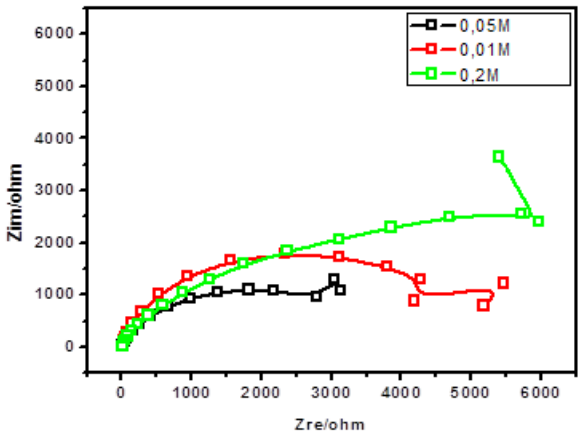

Figure 3.21 : Nyquist graph

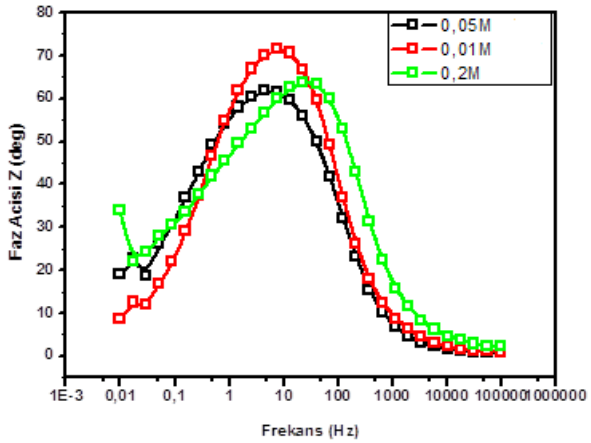

Figure 3.22 : Bode-phase graph

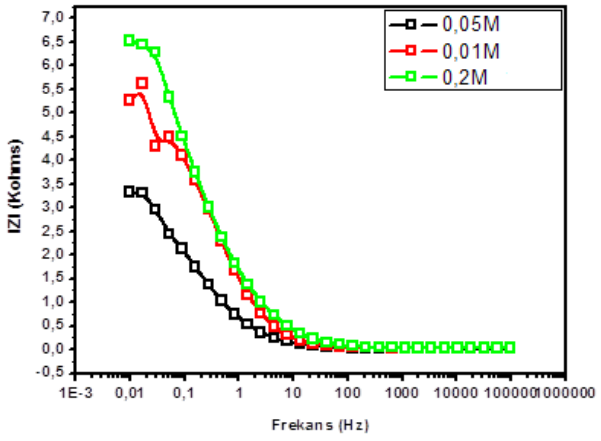

Figure 3.23 : Bode-magnitude graph

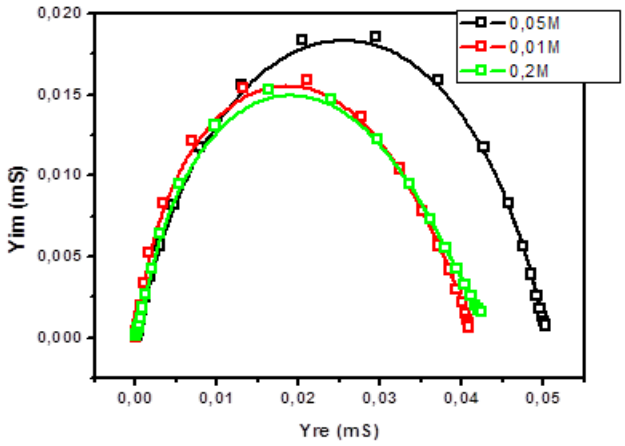

Figure 3.24 : Admittance graph

of higher acid content of the electrodeposition solution. Admittance graph show the same characteristics for lower values.

4. CONCLUSIONS

In conclusion, electrodeposition of CIS was done with pulsed potentiostatic deposition technique. Applied voltage optimization was done before checking other parameters. A new phase for electrodeposition of CIS, wurtzite phase, was assigned which dominates for smaller Se/Cu ratios. Indeed, a competition between wurtzite phase (smooth surfaces) and tetragonal phase (aggregates) was speculated at electrodeposition with both phases present in all samples varying depending on the conditions. Moreover, crystallite size increase up to 17.31 nm was found for high concentrations of acid.

REFERENCES

[1] **Green, M.A., Emery, K., Hishikawa, Y., and Warta, W.** (2010). Solar cell efficiency tables (version 36). *Prog. Photovoltaics*, 18, 346.

[2] **Repins, I., Contreras, M.A., Egaas, B., DeHart, C., Scharf, J., Perkins, C.L., To, B., and Noufi, R.** (2008). 19.9%-efficient ZnO/CdS/$CuInGaSe_2$ solar cell with 81.2% fill factor. *Prog. Photovoltaics: Res. Appl.*, 16, 235.

[3] **Avrutin, V., Izyumskaya, N., and Morkoç, H.** (2011). Semiconductor solar cells: recent progress in terrestrial applications. *Superlattices and Microstructures*, 49, 337.

[4] **Bhattacharya, R.N., Oh, M., and Kim, Y.** (2012). CIGS-based solar cells prepared from electrodeposited precursor films. *Solar Energy Materials & Solar Cells*, 98, 198.

[5] **Contreras, M.A., Egaas, B., Ramanthan, K., Hiltner, J., Swartlander, A., Hasoon, F., and Noufi, R.** (1999). Progress toward 20% efficiency in $Cu(In,Ga)Se_2$ poly-crystalline thin film solar cells. *Prog. Photovoltaics: Res. Appl.*, 7, 311.

[6] **Jiang, J.F.** (2006). Effect of temperature on selenization process of metallic Cu-In alloy precursors. *Thin Solid Films*, 515, 1950.

[7] **Jeyakumar, R., and Ramamurthy, S.** (1994). Electrochemical preparation and characterization of copper indium diselenide thin films. *Materials Research Bulletin*, 29, 195.

[8] **Thouin, L., Massaccesi, S., Sanchez, S., and Vedel, J.** (1994). Formation of copper indium diselenide by electrodeposition. *Journal of Electroanalytical Chemistry*, 374, 81.

[9] **Tzvetkova, E., Stratieva, N., Ganchev, M., Tomov, I., Ivanova, K., and Kochev, K.** (1997). Preparation and structure of annealed $CuInSe_2$ electrodeposited films. *Thin Solid Films*, 311, 101.

[10] **Kemell, M., Ritala, M., Saloniemi, H., Leskelä, M., Sajavaara, T., and Rauhala, E.** (2000). One-step electrodeposition of $Cu_{2-x}Se$ and $CuInSe_2$ thin films by the induced co-deposition mechanism. *Journal of The Electrochemical Society*, 147, 1080.

[11] **De Silva, K.T.L., Priyantha, W.A.A., Jayanetti, J.K.D.S., Chithrani, B.D., Siripala, W., Blake, K., and Dharmadasa, I.M.** (2001). Electrodeposition and characterisation of $CuInSe_2$ or applications in thin film solar cells. *Thin Solid Films*, 382, 158.

[12] **Gujar, T.P., Shinde, V.R., Park, J., Lee, H.K., Jung, K., and Joo, O.** (2009). Characterization of electrochemically grown crystalline $CuInSe_2$ thin films. *Journal of The Electrochemical Society*, 156, E8.

[13] **Chassaing, E., Grand, P.-P., Ramdani, O., Vigneron, J., Etcheberry, A., and Lincot, D.** (2010). Electrocrystallization mechanism of Cu-In-Se compounds for solar cell applications. *Journal of The Electrochemical Society*, 157, D387.

[14] **Ren, T., Yu, R., Zhong, M., Shi, J., and Li, C.** (2011). Microstructure evolution of $CuInSe_2$ thin films prepared by single-bath electrodeposition. *Solar Energy Materials & Solar Cells*, 95, 510.

[15] **Lee, H., Lee, W., Kim, J.Y., Ko, M.J., Kim, K., Seo, K., Lee, D., and Kim, H.** (2013). Highly dense and crystalline $CuInSe_2$ thin films prepared by single bath electrochemical deposition. *Electrochimica Acta*, 87, 450.

[16] **Huang, H., and Lin, C.** (2013). Electrodeposition of compact copper indium diselenide in a stable chloride bath. *Journal of The Electrochemical Society*, 160, H113.

[17] **Hibberd, C.J., Chassaing, E., Liu, W., Mitz, D.B., Lincot, D., and Tiwari, A.N.** (2010). Non-vacuum methods for formtaion of $Cu(In,Ga)(Se,S)_2$ thin film photovoltaic absorbers. *Prog. Photovoltaics*, 18, 434.

[18] **Hernandez-Pagan, E.A., Wang, W., and Mallouk, T.E.** (2011). Teöplate electrodeposition of single-phase p- and n- type copper indium diselenide ($CuInSe_2$) nanowire arrays. *ACS Nano*, 5, 3237.

[19] **Benaicha, M., Benouattas, N., Benazzouz, C., and Ouahab, L.** (2009). Effect of bath temperature and annealing on the formation of $CuInSe_2$. *Solar Energy Materials & Solar Cells*, 93, 262.

[20] **Wolden, C.A., Kurtin, J., Baxter, J.B., Repins, I., Shaheen, S.E., Torvik, J.T., Rockett, A.A., Fthenakis, V.M., and Aydil, E.S.** (2011). Photovoltaic manufacturing: present status, future prospects and research needs. *J. Vac. Sci. Technol. A*, 29, 030801-1.

[21] **Lincot, D.** (2005). Electrodeposition of semiconductors. *Thin Solid Films*, 487, 40.

[22] **Erenturk, B., Gurbuz, S., Corbett, R.E., Claiborne, S.M., Krizan, J., Venkataraman, D., and Carter, K.R.** (2011). Formation of crystalline cadmium selenide nanowires. *Chemistry of Materials*, 23, 3371.

[23] **Linke, W.F. (**1958). Solubilities of Inorganic and Metal Organic Compounds, fourth ed., vol.1., Van Vostrand, Princeton, NJ.

[24] **Palacios-Padros, A., Caballero-Briones, F., and Sanz, F.** (2010). Enhancement in as-grown CuInSe2 film microstructure by a three potential pulsed electrodeposition method. *Electrochemistry Communications*, 12, 1025.

[25] **Valdez, M.H., and Vazquez, M.** (2011). Pulsed Electrodeposition of p-type $CuInSe_2$ thin films. *Electrochimica Acta*, 56, 6866.

[26] **Huang, H., Lin, C., and Chang, W.** (2012). Electrodeposition of CIS films on the Mo back electrodes with different crystallinities. *Electrochimica Acta*, 75, 20.

[27] **Valdez, M., and Vazquez, M.** (2012). Composition, moprhology, and optical properties of $CuInSe_2$ thin films electrodeposited using constant and pulsed potentials. *J. Solid State Electrochem.*, 16, 3825.

[28] **Mandati, S., Sarada, B.V., Dey, S.R., and Joshi, S.V.** (2013). Pulsed electrodeposition of $CuInSe_2$ thin films with morphology for solar cell applications. *Journal of The Electrochemical Society*, 160, D173.

[29] **Valdez, M., Mollar, M., Vazquez, M., and Mari, B.** (2013). Pulsed and potentiostatic electrodeposition of $CuInSe_2$ on gold coated alumina substrates. *J. Appl. Electrochem.*, 43, 619.

[30] **Chandrasekar, M.S., and Pushpavanam, M.** (2008). Pulse and pulse reverse plating- conseptual, advantages and applications. *Electrochimica Acta*, 53, 3313.

[31] **Pungor, E., and Horvai, G.** (1994). A practical guide to instrumental analysis, *ECR Press*, Bosa Roca.

[32] **Peter, L.M.** (2011). Towards sustainable photovoltaics: the search for new materials. *Phil. Trans R. Soc. A*, 369, 1840.

[33] **Kampmann, A., Cowache, P., Lincot, D., and Vedel, J.** (1999). Junction formation studies of one-step electrodeposited $CuInSe_2$ on CdS. *Journal of The Electrochemical Society*, 146, 150.

[34] **Kampmann, A., Sittinger, V., Rechid, J., and Reineke-Koch, R.** (2000). Large area electrodeposition of $Cu(In,Ga)Se_2$. *Thin Solid Films*, 361, 309.

[35] **Norako, M.E., and Brutchey, R.L.** (2010). Synthesis of metastable wurtzite $CuInSe_2$ nanocrystals. *Chem. Mater.*, 22, 1613.

APPENDICES

APPENDIX A: Pulsed Electrodeposition Experiment Data

APPENDIX A

Pulsed Electrodeposition Experiment Data

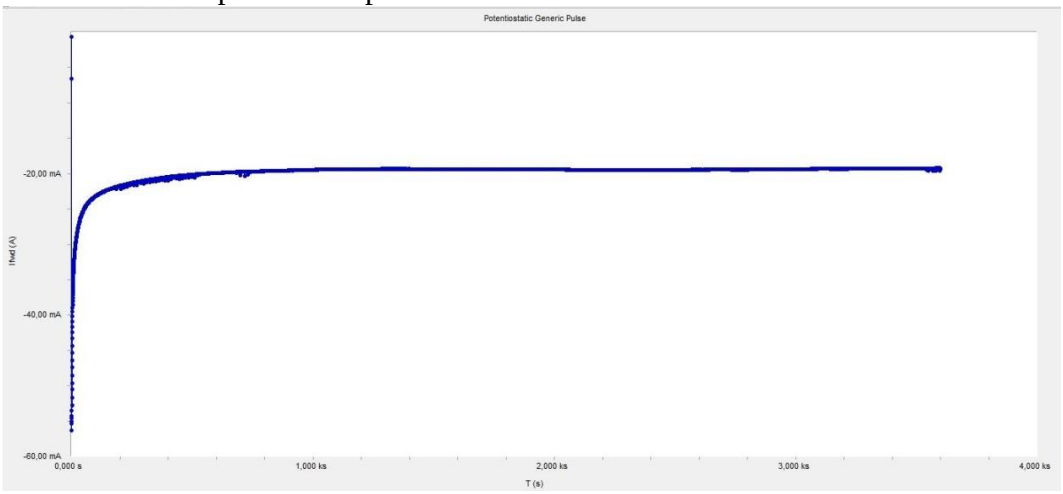

Figure A.1 : -500 mV pulsed electrodeposition experiment data.

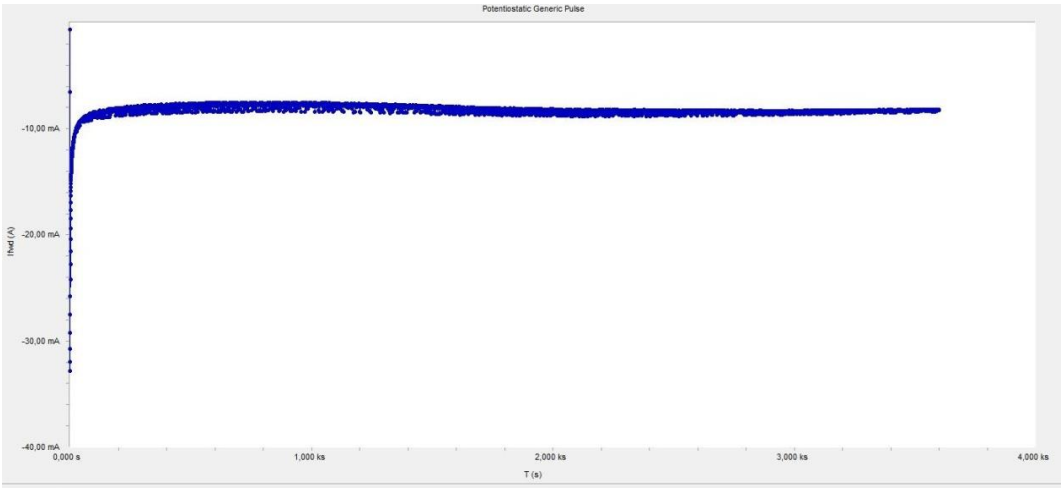

Figure A.2 : -525 mV pulsed electrodeposition experiment data.

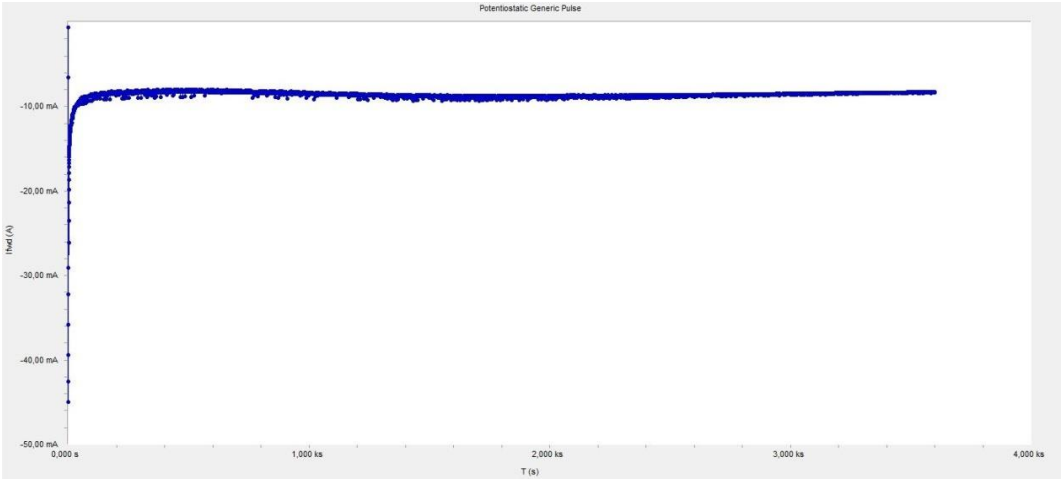

Figure A.3 : -550 mV pulsed electrodeposition experiment data.

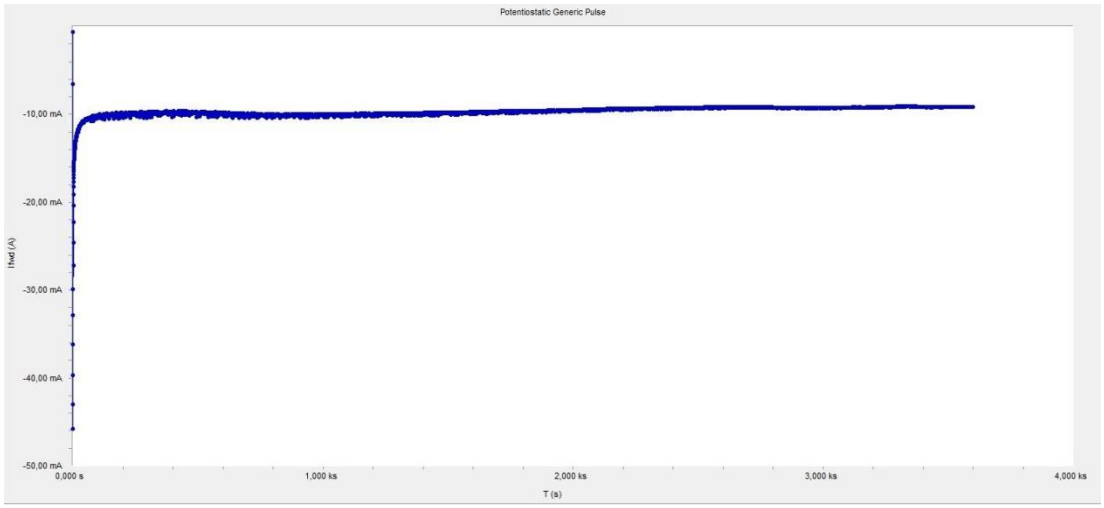

Figure A.4 : -575 mV pulsed electrodeposition experiment data.

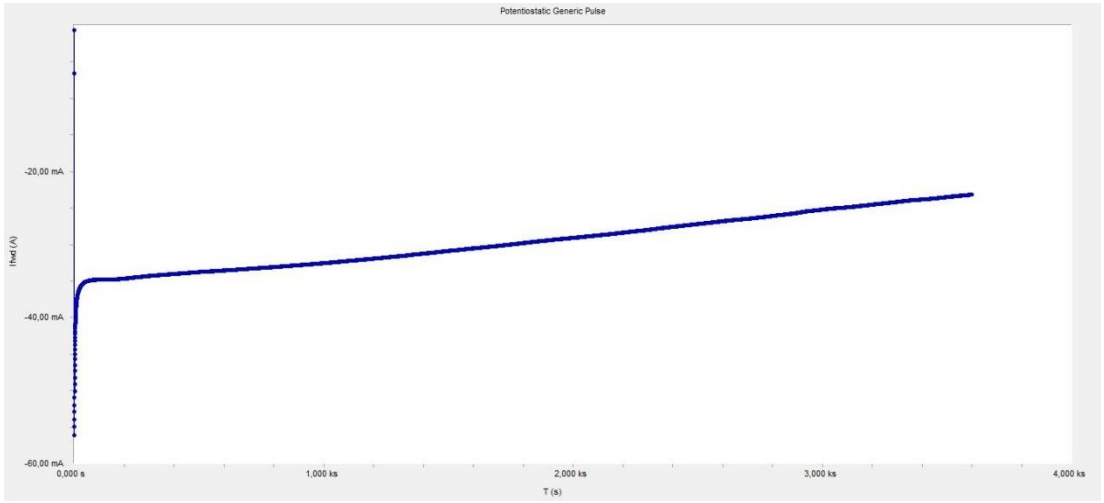

Figure A.5 : -600 mV pulsed electrodeposition experiment data.

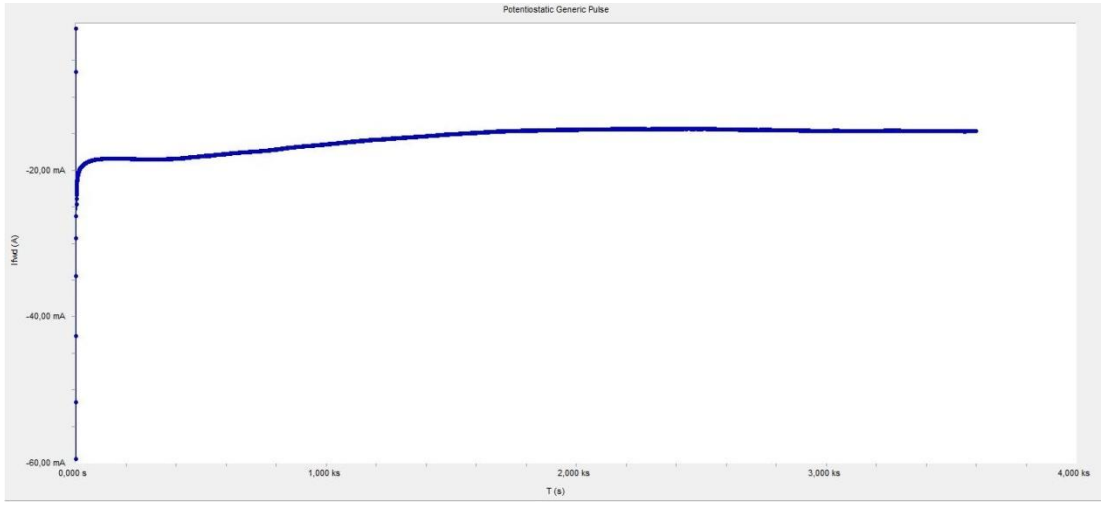

Figure A.6 : -650 mV pulsed electrodeposition experiment data.

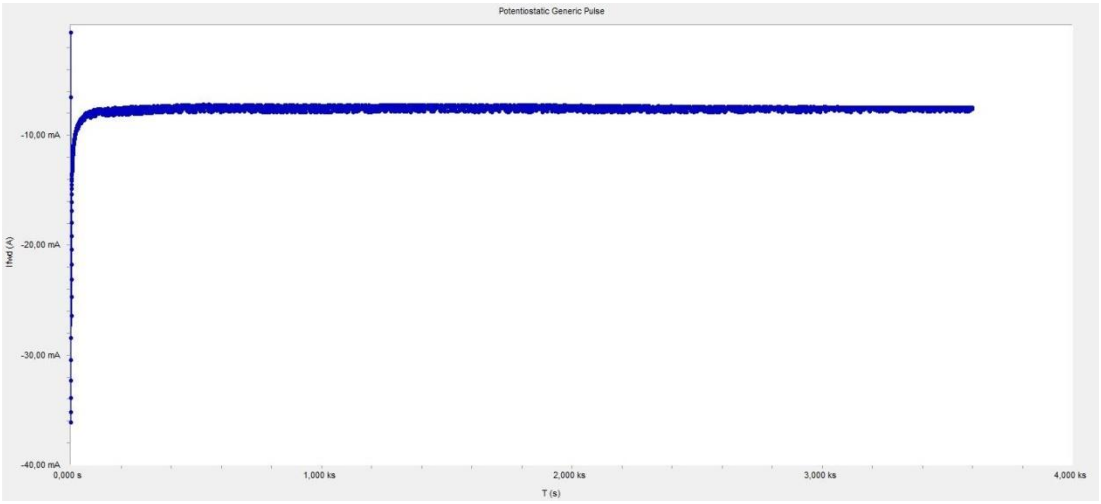

Figure A.7 : 2.125 mM SeO_2 pulsed electrodeposition experiment data.

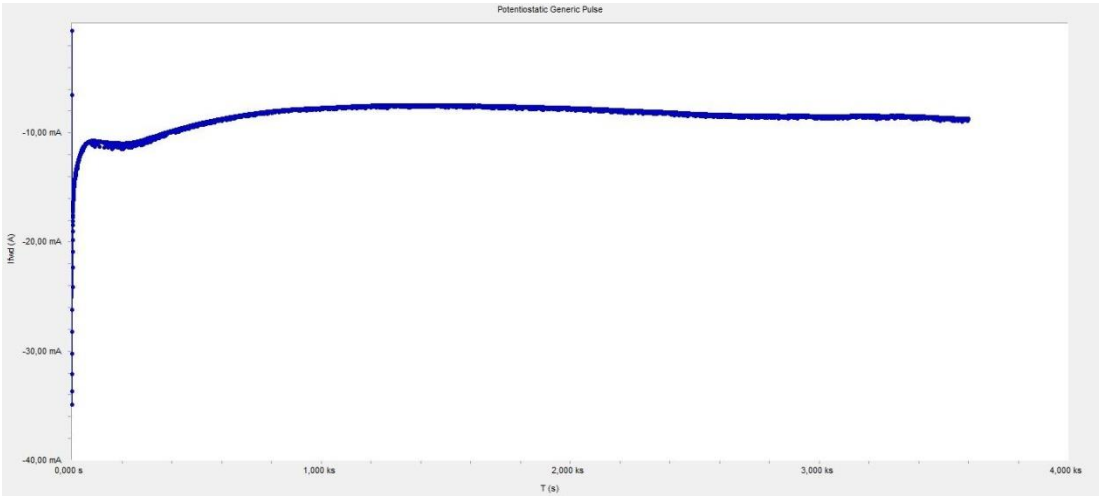

Figure A.8 : 1.275 mM SeO_2 pulsed electrodeposition experiment data.

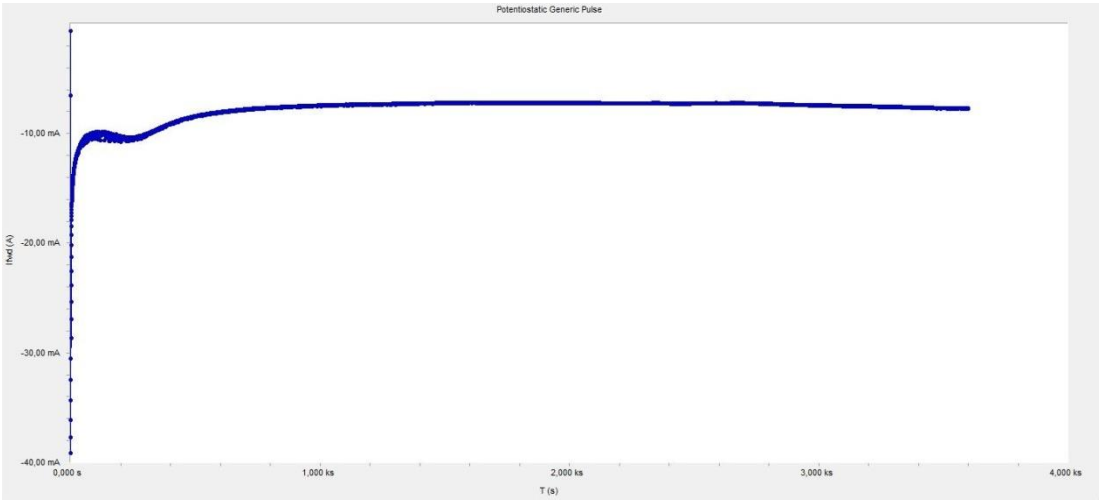

Figure A.9 : 1.25 mM $CuCl_2$ pulsed electrodeposition experiment data.

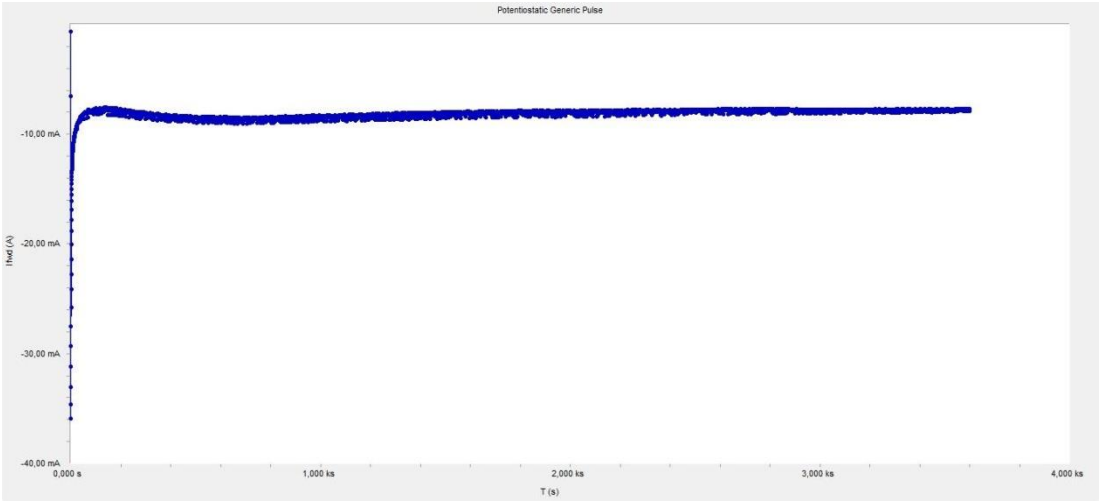

Figure A.10 : 0.75 mM $CuCl_2$ pulsed electrodeposition experiment data.

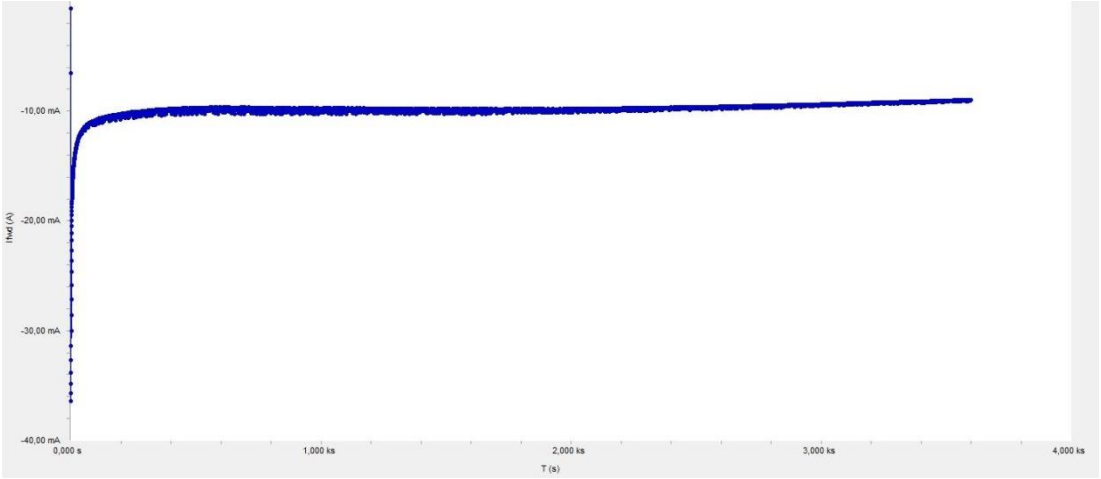

Figure A.11 : 7.5 mM $InCl_3$ pulsed electrodeposition experiment data.

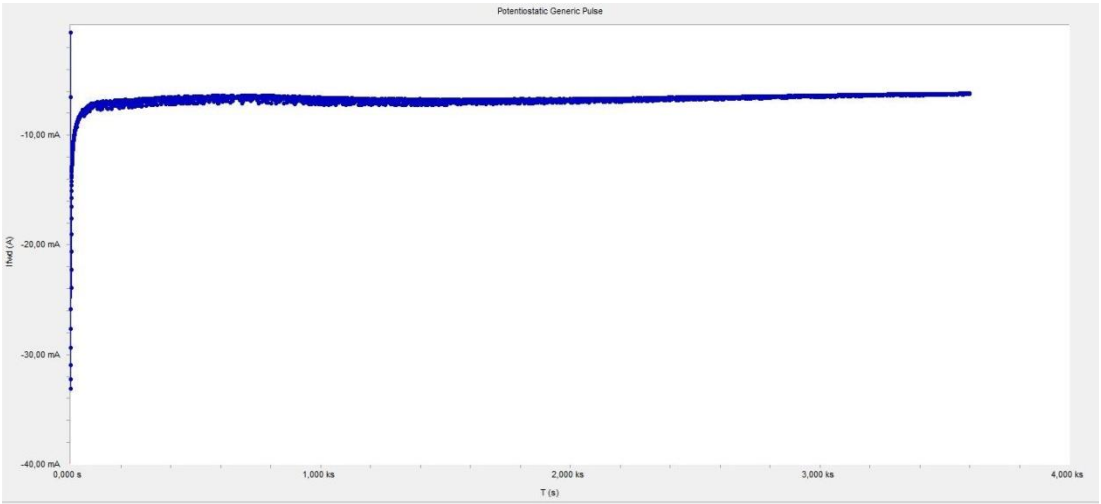

Figure A.12 : 4.5 mM $InCl_3$ pulsed electrodeposition experiment data.

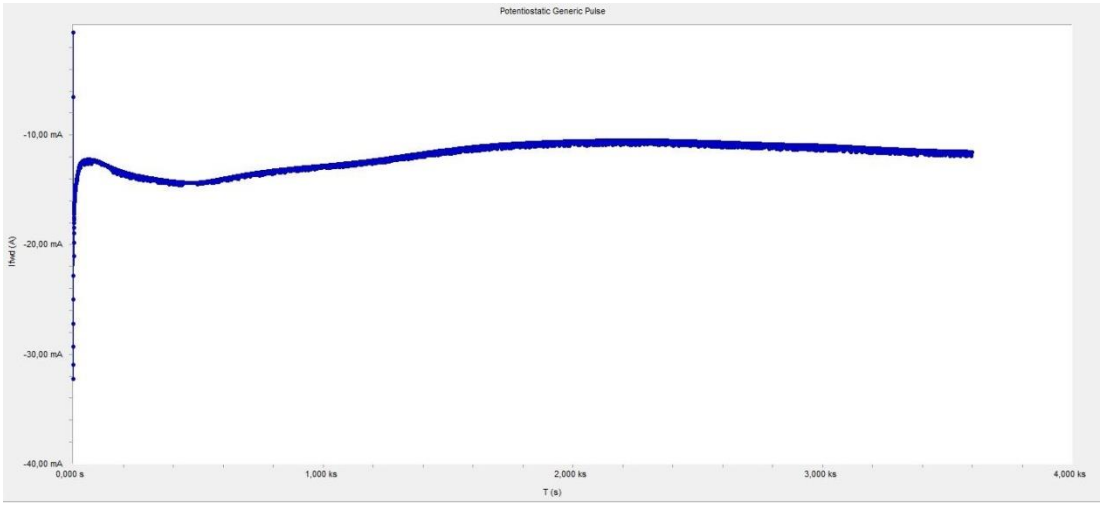

Figure A.13 : 2.125 mM SeO_2 and 1.25 mM $CuCl_2$ pulsed electrodeposition data.

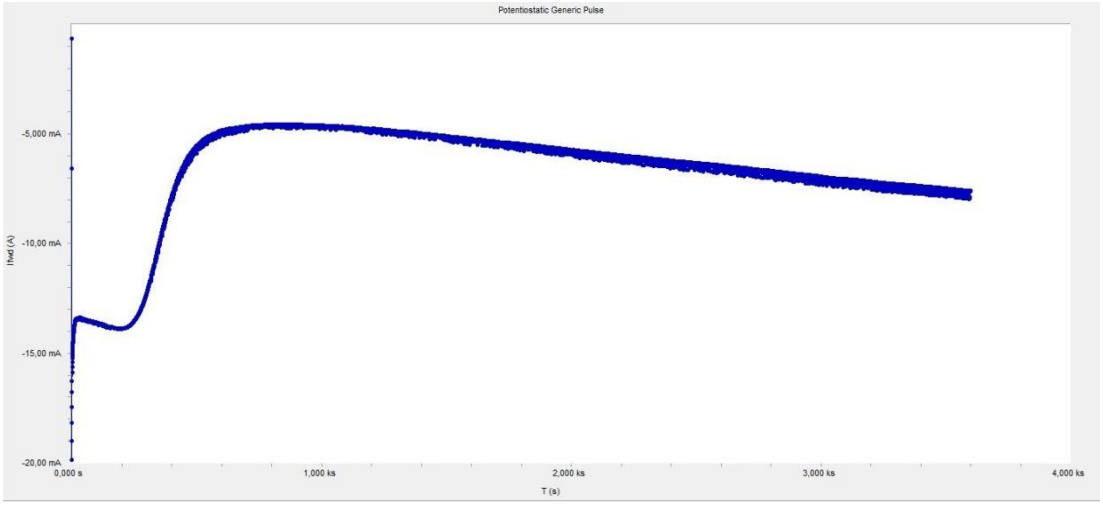

Figure A.14 : 2.55 mM SeO_2 and 1.5 mM $CuCl_2$ pulsed electrodeposition data.

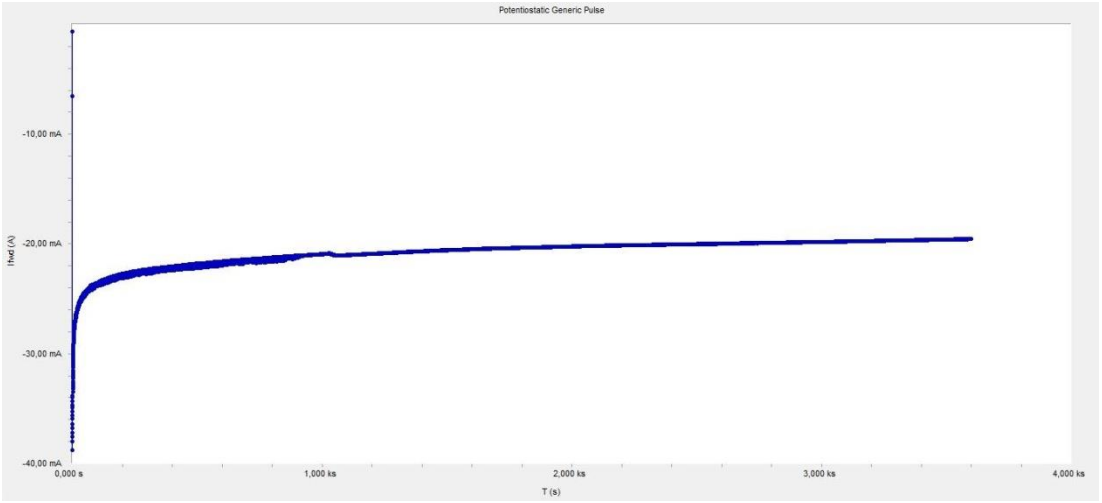

Figure A.15 : 50 ms on-50 ms off time pulsed electrodeposition experiment data.

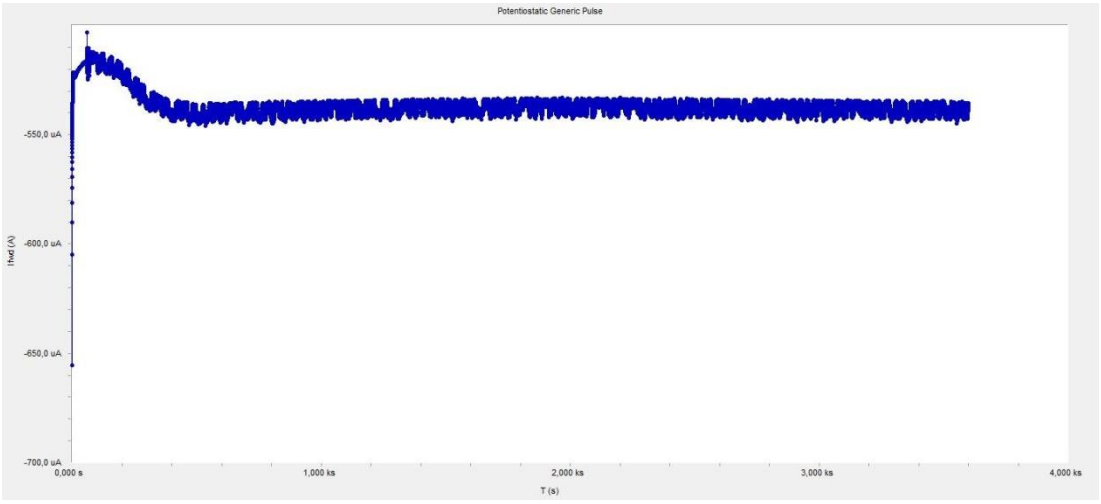

Figure A.16 : 20 ms on-20 ms off time pulsed electrodeposition experiment data.

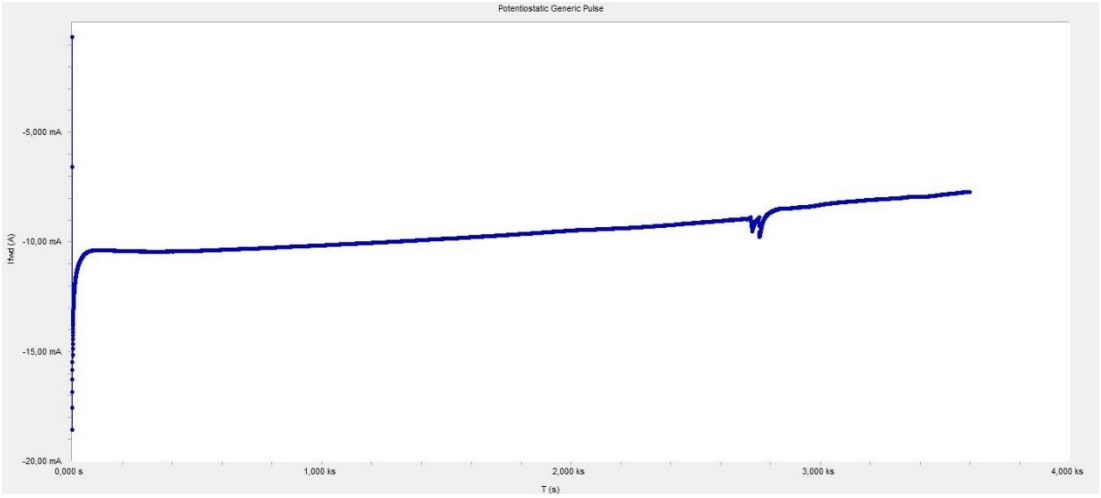

Figure A.17 : 0.05 M HCl pulsed electrodeposition experiment data.

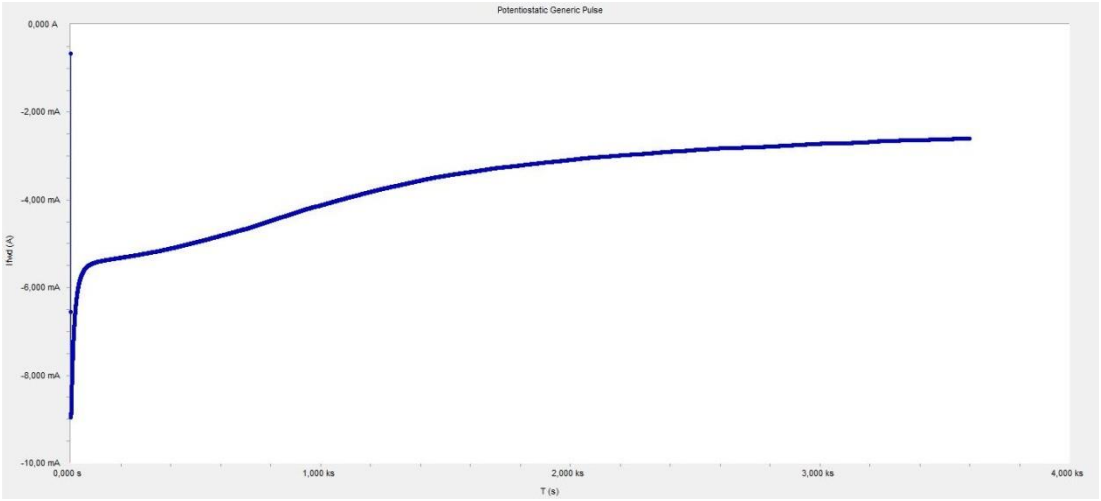

Figure A.18 : 0.01 M HCl pulsed electrodeposition experiment data.

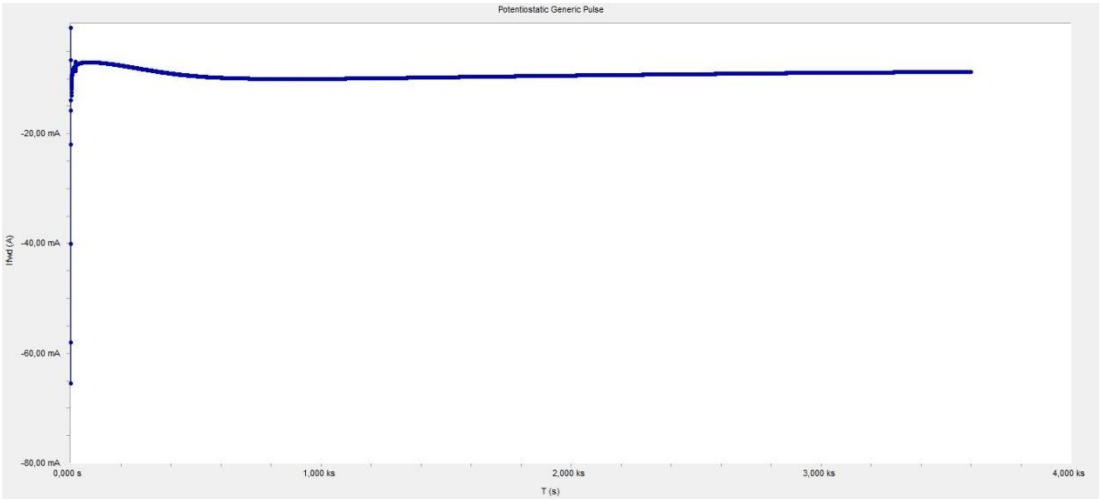

Figure A.19 : 0.5 M HCl pulsed electrodeposition experiment data.

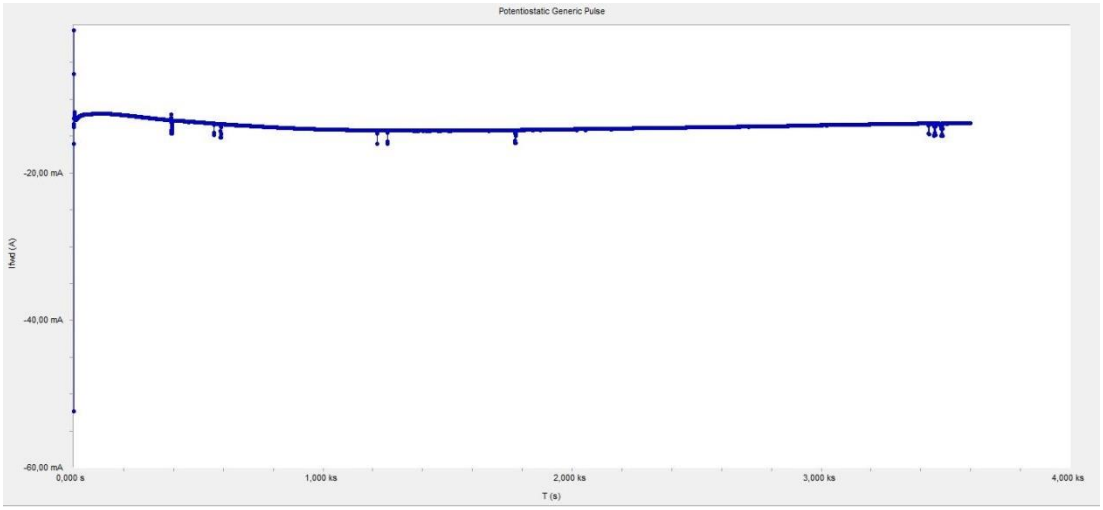

Figure A.20 : 1 M HCl pulsed electrodeposition experiment data.

CURRICULUM VITAE

Name Surname: Serkan GÜRBÜZ

Place and Date of Birth: Bakırköy 03.06.1983

Address: Kadıköy/İSTANBUL

E-Mail: serkan.gurbuz@tubitak.gov.tr

B.Sc.: Bilkent University 2006

List of Publications and Patents:

Benanti, T.L., Chevere-Trinidad, N., Yurt, S., Gurbuz, S., Kalaydjian, A., Swenson, I., and Venkataraman, D. (2007). A contribution to *Applied Physics in the 21st Century, Plastic Solar Cells: An Overview of Thin-Film Technologies for Harvesting Sunlight*.

Erenturk, B., Gurbuz, S., Corbett, R.E., Claiborne, S.M., Krizan, J., Venkataraman, D., and Carter, K.R. (2011). Formation of Crystalline Cadmium Selenide Nanowires. *Chemistry of Materials*, 23, 3371.

Sarioglan, S., Gurbuz, S., Ipeksac, T., Seden, M.G., Erol, M. (2014). Pararosaniline and crystal violet tagged montmorillonite for latent fingerprint investigation. *Applied Clay Science*, 87, 235.

PUBLICATIONS/PRESENTATIONS ON THE THESIS

- **Gurbuz, S., Memis, S., Erol, M., Sarac**, **A. S.** (2014). Electrocrystallization of Copper Indium Diselenide Semiconductor for Solar Cell Applications. *ECS Electrochemistry Letters*, submitted.